Inter-enzyme allosteric regulation of chorismate mutase in *Corynebacterium glutamicum*: Structural basis of feedback activation by Trp

Daniel Burschowsky[1,†,§], *Helen V. Thorbjørnsrud*[1,§], *Joel B. Heim*[1], *Jūratė Fahrig-Kamarauskaitė*[2], *Kathrin Würth-Roderer*[2], *Peter Kast*[2*], *Ute Krengel*[1*]

[1] Department of Chemistry, University of Oslo, NO-0315 Oslo, Norway

[2] Laboratory of Organic Chemistry, ETH Zurich, CH-8093 Zurich, Switzerland

Running title: Shikimate pathway control by inter-enzyme allostery in *C. glutamicum*

KEYWORDS: Corynebacterium glutamicum Cgl0853 and Cg2391; DAHP synthase enzyme catalysis; shikimate metabolic pathway; multi-enzyme complex; X-ray crystal structure

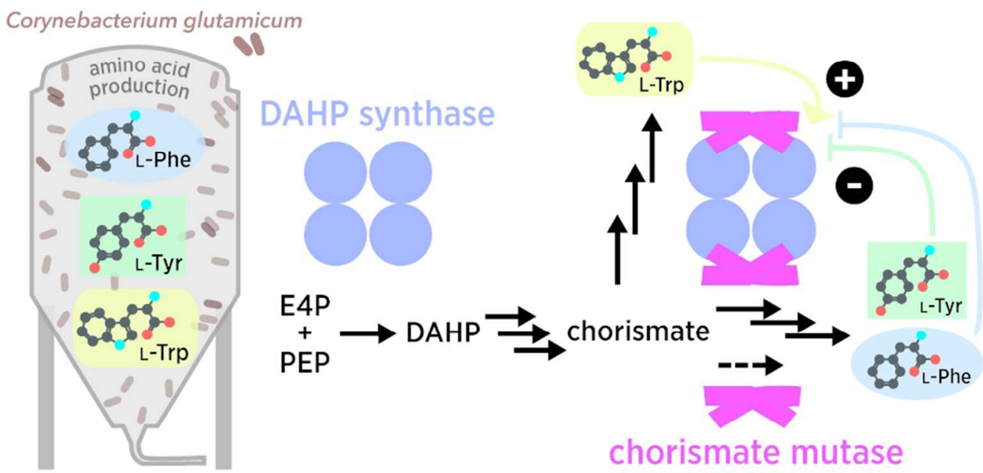

Graphical abstract

ABSTRACT *Corynebacterium glutamicum* is widely used for the industrial production of amino acids, nucleotides, and vitamins. The shikimate pathway enzymes DAHP synthase (CgDS; Cg2391) and chorismate mutase (CgCM; Cgl0853) play a key role for the biosynthesis of aromatic compounds. Here we show that CgCM requires the formation of a complex with CgDS to achieve full activity, and that both CgCM and CgDS are feedback regulated by aromatic amino acids binding to CgDS. Kinetic analysis showed that Phe and Tyr inhibit CgCM activity by inter-enzyme allostery, whereas Trp binding to CgDS strongly activates CgCM. Mechanistic insights were gained from crystal structures of the CgCM homodimer, tetrameric CgDS, and the heterooctameric CgCM-CgDS complex, refined to 1.1 Å, 2.5 Å, and 2.2 Å resolution, respectively. Structural details from the allosteric binding sites reveal that DAHP synthase is recruited as the dominant regulatory platform to control the shikimate pathway, similar to the corresponding enzyme complex from *Mycobacterium tuberculosis*.

INTRODUCTION

The tight control and maintenance of appropriate intracellular concentrations of key metabolites is a general principle across all branches of life. Throughout evolution sophisticated regulatory mechanisms emerged both at the genetic level to vary gene expression *(1)* and at the protein level to control translation and protein turnover and to modulate the function of enzymes through allostery and post-translational modification *(2-9)*. The result is a delicate balance ensuring that the organism is able to produce the essential nutrients and building blocks required for survival, without wasting precious resources once the metabolic needs have been met. One of nature's most powerful strategies for attaining this balance is through feedback inhibition, where a product of a biochemical pathway acts as an inhibitor for the enzymes that are required for its synthesis. This allows cells to dynamically and immediately adapt their metabolic activity to the environment in times of scarcity or abundance. A common mechanism of feedback control is allosteric regulation, whereby effectors bind to a region of an enzyme distant to the active site, resulting in a change in its activity *(2, 6, 10-12)*.

A formidable example for this kind of feedback regulation is observed in the shikimate pathway (Fig. 1), a biosynthetic sequence for production of aromatic amino acids in bacteria, archaea, plants, fungi, and apicomplexan parasites *(13)*, where the activity of several of the enzymes is regulated by allosteric feedback control *(14, 15)*. DAHP synthase (DS) catalyzes the first step in the pathway, an aldol-like condensation of phosphoenolpyruvate (PEP) and D-erythrose-4-phosphate (E4P) to form 3-deoxy-D-*arabino*-heptulosonate-7-phosphate (DAHP). As the first enzyme in the pathway, it serves as a strategic point for feedback regulation *(16)*. An example of this can be seen in the extensively studied model organism *Escherichia coli*, which has three different DSs, each subject to specific inhibition by one of the three aromatic amino acids *(17-19)*.

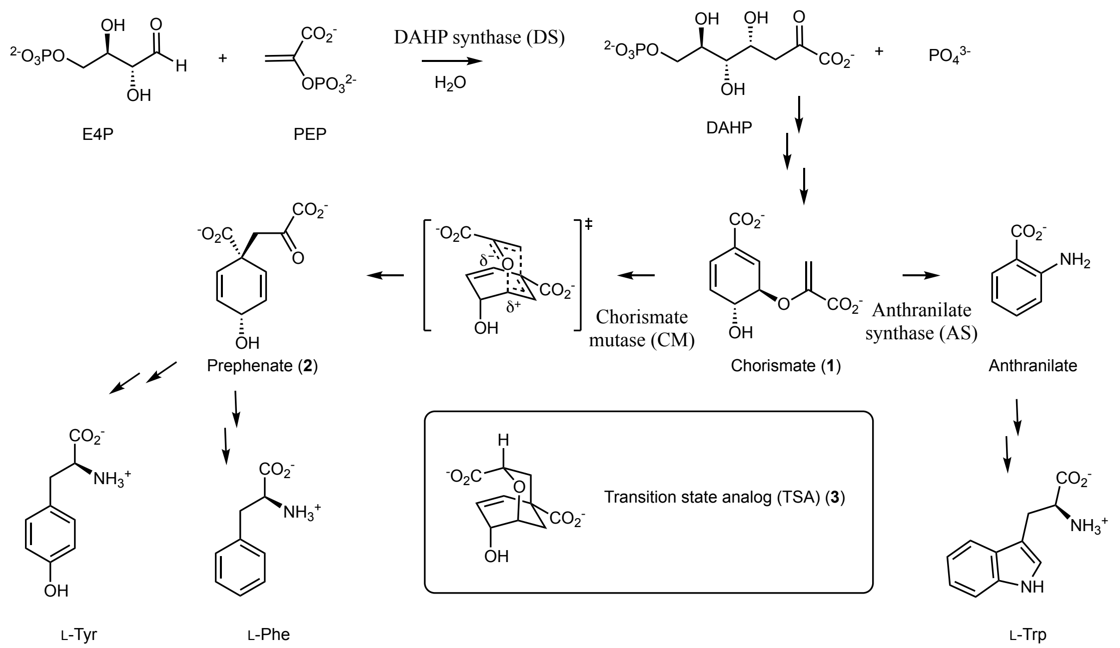

Figure 1. Shikimate pathway. The first enzyme of the metabolic sequence towards aromatic compounds, DAHP synthase, catalyzes the condensation of D-erythrose-4-phosphate (E4P) and phosphoenolpyruvate (PEP) to 3-deoxy-D-*arabino*-heptulosonate-7-phosphate (DAHP). After another six enzymatic steps, the branch point compound chorismate (**1**) is either converted by anthranilate synthase to anthranilate and further to L-Trp, or by chorismate mutase to prephenate (**2**), an intermediate towards L-Tyr and L-Phe biosynthesis. Conversion of **1** to **2** is a pericyclic process with an endo-oxabicyclic transition state exhibiting charge separation at the ether bond to be cleaved. The chair-like transition state is well mimicked by Bartlett's transition state analog (TSA) **3** *(20)*.

Another key enzyme of the shikimate pathway is the central branch point enzyme, chorismate mutase (CM). CM catalyzes the conversion of chorismate (**1**) to prephenate (**2**) *via* a Claisen rearrangement, a rare example of an enzyme catalyzing a pericyclic process *(21, 22)* (Fig. 1). This reaction commits chorismate to the synthesis of L-phenylalanine (Phe) and L-tyrosine (Tyr) as opposed to L-tryptophan (Trp). Due to the unique position at two diverging paths of the aromatic amino acid synthesis, CM is particularly important from a regulatory perspective, again exemplified by the two well-studied bifunctional CMs in *E. coli*, which are sensitive to feedback inhibition by either Tyr or Phe *(23-26)*.

A different strategy for the sophisticated allosteric control of the shikimate pathway has recently been elucidated in *Mycobacterium tuberculosis*. Instead of bifunctional CMs, the open reading frame Rv0948 encodes a mono-functional CM (MtCM) that is utilized for the cytoplasmic synthesis of Tyr and Phe in *M. tuberculosis* H37Rv. Interestingly, MtCM shows only modest activity on its own compared to typical wild-type CMs *(27-31)*. However, upon formation of a heterooctameric complex with DAHP synthase (MtDS, encoded by Rv2178c) (Fig. 2), crucial MtCM active site residues are repositioned, and the catalytic CM activity increases by more than a hundred-fold *(32)*.

MtCM-MtDS complex formation plays a key role as a regulatory feature of the shikimate pathway in *M. tuberculosis*. The DS activity of MtDS is synergistically inhibited by the end products of the pathway (Phe, Tyr, and Trp), whereas the CM activity of the MtCM-MtDS complex, but not of MtCM alone, is synergistically inhibited by Phe and Tyr *(32-36)*. In an evolutionary study on the MtCM-MtDS complex, we could show that the activation factor by MtDS of MtCM variants is directly correlated with their response to the feedback inhibitors Tyr and Phe *(37)*.

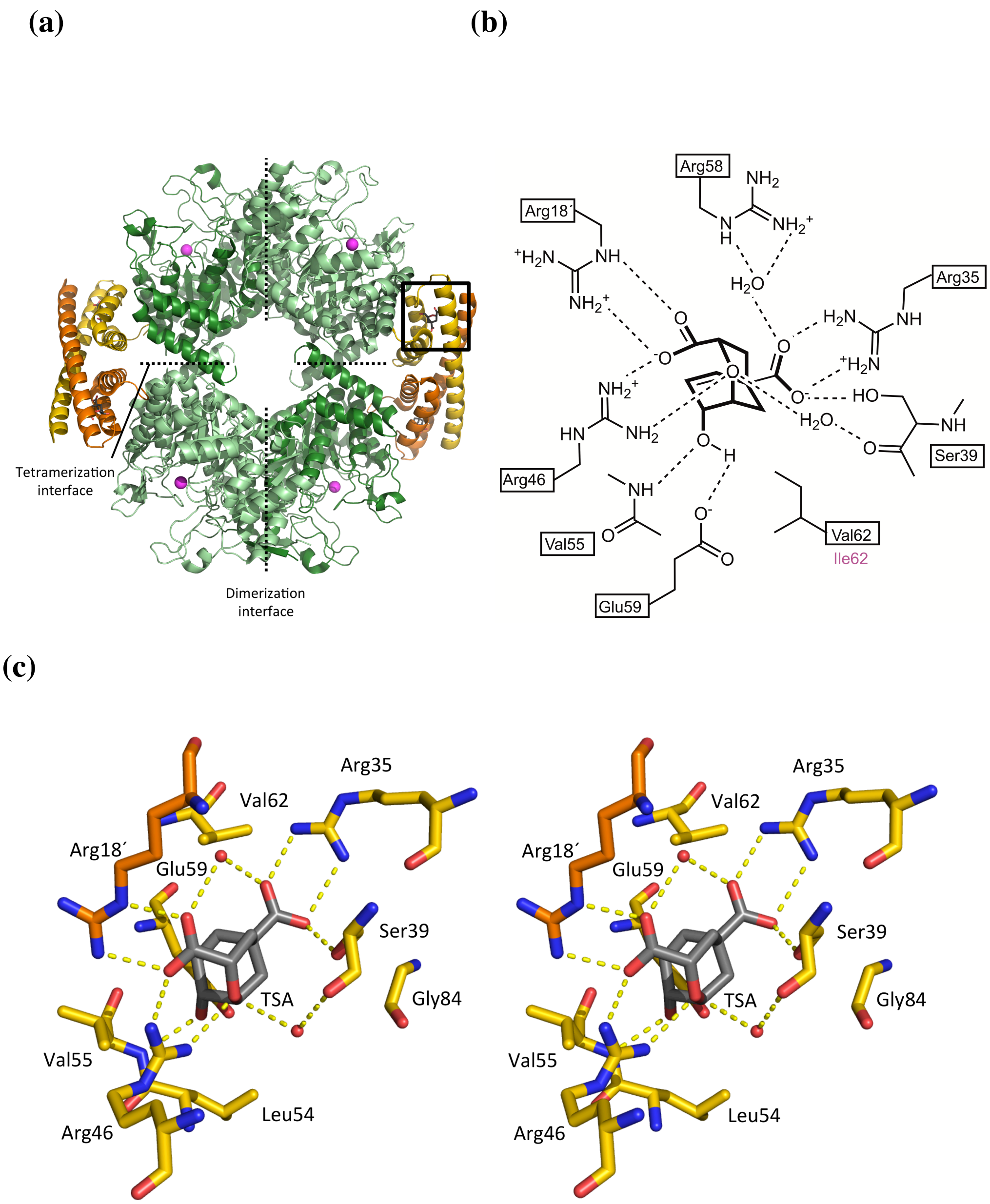

Figure 2: Complex formation with MtDS preorganizes the MtCM active site for catalysis. (a) Cartoon illustration of the active MtCM-MtDS heterooctameric complex (PDB: 1W1A *(32)*). MtCM is colored in yellow and orange, the transition state analog (TSA) **3** in dark grey, and MtDS in shades of green to emphasize individual subunits.

Dimerization and tetramerization interfaces of MtDS are indicated. The box highlights the location of one of the four active sites depicted in b and c. (b) Schematic representation of the CM active site with TSA bound. Boxed residues refer to MtCM, while Ile62 marked in pink refers to the corresponding residue in CgCM. (c) Stereo image of the MtCM active site in the MtCM-MtDS complex, with TSA in dark grey. Arg18´ is labeled with a prime and colored in orange to show that this residue originates from the other protomer of the dimeric MtCM.

All inhibitor binding sites are found in MtDS, distant from the MtCM-MtDS interface *(36)*. Despite the distance, the presence of these inhibitors induces complex dissociation, as established by several biochemical and biophysical experiments *(35, 36)*. This mode of indirectly regulating CM activity was only recently appreciated and characterized, and has been designated inter-enzyme allostery *(36)*. Curiously, binding of the effectors to the complex only leads to negligible structural rearrangements of MtCM and MtDS, possibly causing tiny subunit misalignments that destabilize the heterooctameric assembly *(36)*. It was also proposed that feedback inhibition may be the result of a change in dynamics of the enzymatic complex *(33, 35, 36, 38)*. This is in keeping with a modern interpretation of allosteric regulation, suggesting that allosteric signaling can be driven by shifting populations of conformational ensembles, without necessitating clear structural rearrangements *(6, 39-44)*.

Previous data and phylogenetic investigations indicate that the interaction between CM and DS could be a feature of shikimate pathway regulation unique to a few taxonomic orders within the bacterial class *Actinobacteria*, such as the *Corynebacteriales* *(32, 36)*.

Corynebacterium glutamicum is a non-pathogenic representative from the bacterial order *Corynebacteriales* and is used for the large-scale industrial production of amino acids, vitamins, and other food additives *(45-48)*. Unlike *M. tuberculosis*, *C. glutamicum* ATCC 13032 has two genes coding for DS enzymes, a Type I DS (named NCgl0950 *(45)* or *cg1129 (49)*) and a Type II DS (NCgl2098 *(45)* or *cg2391 (49)*). Only the Type II DS is required for *C. glutamicum* growth in minimal media, indicating that only this enzyme is vital for amino acid production *(50)*. The sequence identity between the CM of *C. glutamicum* (CgCM) and MtCM is 59%, and it is 65% between the Type II DS of *C. glutamicum* (CgDS) and MtDS. It has also been shown that MtDS can heterologously increase the activity of CgCM, which suggested that CM-DS complex formation plays a similar role in *C. glutamicum* as in *M. tuberculosis (32)*. When the *C. glutamicum* enzymes were first studied (before *Brevibacterium flavum* was reclassified as *C. glutamicum (51)*), it was not possible to detect any CM activity in the absence of DS, pointing to a dramatic activating effect upon complex formation *(52, 53)*. However, recent publications stated that CgDS did not enhance the catalytic activity of CgCM *(54, 55)*. Thus, there is currently contradictory information in the literature regarding the regulation at one of the key branch points in the metabolism of this biotechnologically important bacterium.

Here, we use kinetic and structural approaches to elucidate similarities and differences between the CM-DS systems of *C. glutamicum* and *M. tuberculosis*. In particular, we were interested whether CgCM-CgDS is also subject to inter-enzyme allosteric regulation, and how its molecular mechanism compares to that previously established for MtCM-MtDS. Our findings established the crucial importance of CgCM-CgDS complex formation for controlling CgCM activity. As an additional feature we discovered cross-pathway activation by Trp under physiological conditions, thus expanding the toolkit accessible to CgCM, *via* the principal regulatory platform of the shikimate pathway in *C. glutamicum*.

MATERIALS AND METHODS

Assembly of gene expression plasmids

For the production of CgCM, we first used plasmid pKCGCM-HC *(32)*, expressing the entire reading frame of the originally annotated *C. glutamicum* gene Cgl0853, provided with a 3' appended sequence encoding a C-terminal His_6-tag. However, after gene expression and purification, this tagged CgCM variant showed two subpopulations of N-terminally degraded protein, shorter by 20 and 22 amino acids, as identified by LC-MS. Upon further scrutiny of the primary sequence (for a discussion about the most probable start codon, see *(32)*), the gene was recloned, this time using the third methionine (annotated as Met13 in gene Cgl0853) as the start codon, resulting in plasmid pKCGCM-H (4807 bp) *(32)*. We regard this smaller 90 amino acid CgCM protein variant (shorter by 12 N-terminal residues relative to the annotated reading frame), which is devoid of any purification tag and which did not show any significant proteolytic degradation, as the native form of CgCM and we consequently used it throughout this work.

Plasmid pKCGDS-HN encodes an N-terminally His_6-tagged version of the open reading frame of gene Cgl2178 (*i.e.*, with Met–His_6–Ser–Ser–Gly fused to the start methionine). This CgDS gene construct was assembled after PCR amplification of chromosomal DNA of *C. glutamicum* ATCC 13032 (see *(32)* for DNA source and preparation). The PCR (94°C for 2 min; 25 cycles of 94°C for 30 s, 58.3°C for 30 s, 72°C for 90 s; followed by 72°C for 10 min) employed oligonucleotides 332-DSCG3N-S (TTGTGTCATATGCACCATCATCATCATCATTCTTCTGGTATGAGTGGACAGTTGATATCCCTAAA) and 333-DSCG4-N (TAGAACACTAGTTATTAGTTACGCAGCATTTCTGCAACG) resulting in a 1,442 bp PCR fragment. After digestion with *Nde*I and *Spe*I, the 1,424 bp PCR fragment was ligated to the 4,529 bp *Nde*I-*Spe*I fragment of vector pMG211 *(30)* yielding CgDS expression plasmid pKCGDS-HN (5953 bp).

The DNA sequences of the cloned genes were confirmed over their entire length by DNA sequencing on an ABI Prism 3100 DNA Sequencer using two (for the CgCM gene) and four (for the CgDS gene) custom made sequencing primers (Microsynth AG, Balgach, Switzerland).

Protein production and purification

Plasmids pKCGCM-H and pKCGDS-HN were used to overproduce the native (untagged) CgCM and N-terminally His_6-tagged CgDS, respectively, in *Escherichia coli* KA13 (a strain deficient in CMs) *(28, 56)*. A single colony of freshly transformed cells was grown overnight in 5 mL LB medium containing 100 μg/mL sodium ampicillin (LB-amp), and aliquoted for frozen stocks after adding glycerol to a concentration of 10% (v/v).

A 50 mL LB-amp pre-culture was inoculated using scrapes of frozen stock, and grown overnight at 37 °C. The LB-amp main culture (2x 1 L) was inoculated to an OD_{600nm} of 0.05 and incubated at 110 rpm in a shaking incubator at 30 °C until an OD_{600nm} of 0.5 was reached. Then, gene expression was induced by adding IPTG to a final concentration of 0.5 mM. The production culture was incubated at 30 °C for approximately 18 h, centrifuged at 6500 × *g* for 20 min (4 °C), and the cell pellet was frozen before further processing.

For CgCM, the pellet was resuspended in 20 mM sodium phosphate buffer (pH 8.0), containing 150 μM PMSF and *cO*mplete protease inhibitor (Roche). Cells were homogenized by two passes through a high-pressure homogenizer and subsequently pelleted at 48000 × *g* for 30 min (4 °C). The lysate was loaded on a 5 mL HiTrap XL SP ion exchange column (GE Healthcare) and eluted with a gradient from 0 – 500 mM NaCl. Homogeneous fractions were pooled, concentrated (Vivaspin MWCO 3k), and further purified on a Superdex 75 300/10 column (GE Healthcare), run with 20 mM Bis-Tris propane (1,3-bis(tris(hydroxymethyl)methylamino)propane) (pH 7.5), 150 mM NaCl. Pure fractions were concentrated after addition of 0.01% NaN_3 and stored at -20 °C.

For CgDS, the pellet was resuspended in 50 mM Tris-HCl buffer (pH 8.2), containing 300 mM NaCl, 5% glycerol, 2 mM β-mercaptoethanol, 20 mM imidazole, 150 μM PMSF and *cO*mplete protease inhibitor (Roche). Cells were homogenized by two passes through a high-pressure homogenizer and subsequently pelleted at 48000 × *g* for 30 min (4 °C). The lysate was loaded on a 5 mL Ni-NTA column (GE Healthcare) and eluted with a gradient from 20 – 500 mM imidazole using a buffer containing 50 mM Tris-HCl (pH 8.0), 300 mM NaCl, 150 μM PMSF, 5% (v/v) glycerol, 100 μM $MnCl_2$, and 200 μM PEP. Fractions containing CgDS were pooled and dialyzed twice against 20 mM Tris-HCl (pH 7.0), 1 mM β-mercaptoethanol, 100 μM $MnCl_2$, and subsequently loaded on a 5 ml HiTrap XL Q column (GE Healthcare) and eluted with a gradient from 0 – 500 mM NaCl. Homogeneous fractions were pooled, concentrated (Vivaspin MWCO 30k), and further purified on a Superdex 200 300/10 column (GE Healthcare), run with 20 mM Bis-Tris propane (pH 7.5), 150 mM NaCl, 0.5 mM TCEP (tris(2-carboxyethyl)phosphine), 100 μM $MnCl_2$, 200 μM PEP. Pure fractions were concentrated after addition of 0.01% NaN_3 and stored at -20 °C.

Enzyme activity assays

Chorismate was produced using a previously published protocol *(57)*. *In vitro* CM activity assays were conducted at 30°C as previously described *(32)*; briefly, the initial velocities (v_0) needed for fitting to the Michaelis-Menten equation $v_0 = k_{cat}\cdot[E]\cdot[S]/(K_m+[S])$ were obtained by continuously monitoring the consumption of chorismate at 274 nm ($\varepsilon_{274\ nm}$ = 2630 M^{-1} cm^{-1}) or 310 nm ($\varepsilon_{310\ nm}$ = 370 M^{-1} cm^{-1}) over a chorismate concentration range from 500 μM to 3 mM. The k_{cat}/K_m of CgCM was determined at 310 nm in 50 mM Bis-Tris propane (pH 7.5), with a CgCM concentration of 950 nM. An apparent k_{cat}/K_m of CgCM-CgDS was determined at 310 nm in Bis-Tris propane (pH 7.5), 0.5 mM TCEP, 100 μM $MnCl_2$, 200 μM PEP, with CgCM and CgDS concentrations held at 50 and 1000 nM, respectively, while the chorismate concentration was varied between 100 μM and 2.6 mM.

For the assays measuring the effect of aromatic amino acids, effector concentrations were standardized to 25 μM in all cases, CgCM concentration was 100 nM and CgDS concentration was 1000 nM, and chorismate (at 100 μM) consumption was followed at 274 nm.

Crystallization

Crystallization was generally performed and optimized in hanging-drop setups, except for the CgCM-CgDS complex, where sitting-drop setups were used following robotic screening. CgCM was crystallized by adding 1 μL protein solution (7.5 mg/mL) to 1 μL well-solution (100 mM NH_4 formate (pH 6.6), 100 mM KSCN, 30% PEG 2000 MME), at 20 °C. CgDS was crystallized by adding 1 μL protein solution (10.0 mg/mL) to 1 μL well-solution (100 mM Tris-Bicine buffer (pH 8.7), 13% MPD, 13% PEG 1000, 13% PEG 3350, 2% tri-ethylene glycol, 200 μM PEP, 100 μM $MnCl_2$), at 4 °C. For the Trp complex, the crystals were soaked by adding 1 μL 2 mM Trp to the drop at 25 °C and incubating for 30 min before freezing the crystals.

Crystallization of the CgCM-CgDS-TSA complex was facilitated by microseeding. Seeds were prepared by crushing poorly diffracting crystals in the drop with a glass rod, and transferred to 50 μL of the reservoir solution (100 mM Na-HEPES (pH 7.5), 200 mM $LiSO_4$, 25% PEG 3350). A glass bead was added and the suspension was mixed by vortexing for 2 min. The resulting seed stock was diluted up to 1:1000. For crystallization, 0.13 mM CgCM and 0.12 mM CgDS were mixed and incubated at 25 °C for 30 min with a few flakes of solid transition state analog (TSA) **3** (8-hydroxy-2-oxa-bicyclo[3.3.1]non-6-ene-3,5-dicarboxylic acid) *(20)*. After incubation, crystallization experiments were set up with an Oryx 4 robot (Douglas Instruments, UK), mixing 0.15 μL protein solution, 0.15 μL 1:10 seed stock, and 0.3 μL well solution into a Swissci 2 sitting drop 96-well plate (and 50 μL reservoir solution). Well-diffracting crystals were obtained in 100 mM imidazole/MES buffer (pH 6.5), 30 mM each of ethylene glycol mix (equal amounts of di-ethylene glycol, tri-ethylene glycol, tetra-ethylene glycol, penta-ethylene glycol), 15% glycerol, and 15% PEG 4000. TSA was produced by Dr. Rosalino Pulido according to a previously published procedure *(58)*.

Data collection, structure determination, and refinement

All data were collected at the ESRF, at beam line ID-29. The diffraction images were processed with *XDS* *(59)*, and the resulting data merged with *AIMLESS* *(60)*. 5HUC and 5HUE data sets were processed without averaging Friedel pairs to include anomalous information in the refinement. The resolution cut-off for the crystallographic data was chosen in accordance with the significance test employed by *XDS* *(59)*. Instead of R_{merge}. we used the new gold standard for data quality control, $CC_{1/2}$ *(60-63)*. The structure was determined by molecular replacement (MR) with the program *Phaser* *(64)*. For CgCM, terminally truncated MtCM (PDB-ID: 2VKL *(32)*) was used as MR model. For CgDS, a suitable MR model was built from MtDS (PDB-ID: 2B7O *(65)*) using *CHAINSAW* *(66)*. For the CgCM-CgDS complex, the tetrameric MtDS as derived from the MtCM-MtDS complex (PDB-ID: 2W1A *(32)*) was used as a model for MR, and CgCM was subsequently built into the density manually. The structures were refined by alternating manual model building and automatic refinement using *Coot* *(67)* and *REFMAC5* *(68)*, respectively. All programs from data merging to final structure polishing were part of the *CCP4* 6.5.019 package *(69)*. A summary of the data collection and refinement statistics is given in Table 1. The atomic coordinates and structure factors have been deposited at the Protein Data Bank *(70, 71)* with accession codes 5HUB, 5HUC, 5HUD, and 5HUE. Buried surface areas were calculated with the PDBe PISA webserver *(72)*. Structure images, superimpositions, and angle measurements were prepared using different versions of Pymol (Schrödinger, LLC), and reaction schemes were created with ChemDraw Professional 15.0 (PerkinElmer Informatics, Inc.).

Table 1: Data collection and refinement statistics

	CgCM	CgDS	CgDS w/ Trp soak	CgCM+CgDS w/ TSA
X-ray source	ID29, ESRF	ID29, ESRF	ID29, ESRF	ID29, ESRF
Wavelength (Å)	0.9791	0.9763	0.9763	0.9724
Space group	$C2$	$P6_222$	$P6_222$	$P2_1$
Unit cell parameters				
a (Å)	82.9	109.8	109.2	117.6
b (Å)	24.6	109.8	109.2	110.5
c (Å)	38.6	279.3	279.9	134.7
α (°)	90	90	90	90
β (°)	99.4	90	90	101.4
γ (°)	90	120	120	90
Resolution (Å)	40.9-1.1 (1.13 - 1.06)	95.1-2.5 (2.60 - 2.45)	37.0-2.6 (2.80 - 2.64)	132.0-2.2 (2.28 - 2.15)
$I/\sigma(I)$	9.0 (0.4)	14.0 (0.6)	9.4 (0.4)	4.8 (0.6)
No. of reflections				
Observed	131255 (8199)	473980 (54009)	517828 (83525)	539068 (69033)
Unique	30562 (2733)	36845 (5163)	29830 (4679)	179323 (26905)
Redundancy	4.3 (3.0)	12.9 (10.5)	17.4 (17.9)	3.0 (2.6)
Completeness (%)	87.9 (49.2)	97.9 (87.0)	99.8 (99.3)	97.7 (91.2)
$CC_{1/2}$[a]	99.8 (39.2)	99.9 (59.6)	99.8 (31.6)	98.7 (95.4)
Wilson B factor (Å^2)	16.0	73.8	72.7	19.5
R_{work} / R_{free}[b]	0.17 / 0.22	0.24 / 0.25	0.25 / 0.28	0.25 / 0.30

rmsd bond length (Å)	0.019	0.007	0.007	0.011
rmsd bond angle (°)	2.01	1.18	1.26	1.53
Average *B* factor (Å^2)				
Backbone	18.1	112.0	107.8	32.1
Side chain + water	24.9	114.4	111.2	36.1
All atoms	22.0	113.2	109.5	34.3
Number of atoms	833	3564	3571	18279
Protein	716	3483	3456	16628
Ligand(s)	n.a.	26	26	148
Solvent/Buffer (H_2O)	117 (111 H_2O)	55 (21 H_2O)	89 (21 H_2O)	1503 (780 H_2O)
Ramachandran (%)				
Favored	98.5	94.6	95.5	96.9
Allowed	0.0	4.9	3.8	2.9
Outliers	1.5	0.5	0.7	0.2
PDB ID	5HUB	5HUC	5HUE	5HUD

[a]According to *(60, 61)* [b] $R = \Sigma||F_o|-|F_c||/ \Sigma |F_o|$ where F_o and F_c are the observed and calculated structure factors, respectively. R_{free} is R calculated for 5% randomly selected reflections, which were omitted from the refinement. Values in parentheses refer to the highest resolution shell.

RESULTS

Enzymatic activation of CgCM by CgDS

To address the contradictions within the literature about whether or not CgCM is activated by CgDS, we produced CgCM in its native (untagged) form and CgDS with an N-terminal His_6-tag (see *Materials and Methods* for details). These protein formats are identical to the ones investigated previously for the *M. tuberculosis* system, where it was shown that the tag does not interfere with DS activity or CM activation *(36)*. Enzymatic activity was determined by following the conversion of chorismate by CgCM alone and in the presence of CgDS.

The K_m of CgCM is too high (>3000 μM) to obtain a meaningful fit of the experimentally attainable data for deriving k_{cat} and K_m from the Michaelis-Menten equation. However, it was still possible to accurately determine the ratio k_{cat}/K_m for isolated native CgCM as 110 M^{-1} s^{-1} (Table 2). This value is within the same order of magnitude as the k_{cat}/K_m previously measured for N-terminal His-tagged variants of CgCM (370 M^{-1} s^{-1} and 390 ± 60 M^{-1} s^{-1}) *(32, 54)*, and 3-4 orders of magnitude below that of typical DS-independent CMs *(27-31)*. Upon addition of CgDS, CgCM catalysis can be boosted 180-fold, proving a dramatic activation effect similar to that observed for the *M. tuberculosis* system (Table 2). This is in stark contrast to the data of the CgCM-CgDS study published recently, where no stimulation of CM activity was observed *(54)*.

Table 2: Apparent catalytic parameters for the conversion of chorismate to prephenate

	k_{cat}/K_m (M^{-1} s^{-1})	Fold activation by DS
CgCM[a]	111 ± 7	
CgCM-CgDS[a]	(2.01 ±0.01) × 10^4	182 ± 12
MtCM[b]	1750 ± 90	
MtCM-MtDS[b]	(2.4 ±0.6) × 10^5	140 ± 35

[a] Measured in 50 mM BTP+, pH 7.5, at 50 nM CgCM and 1000 nM CgDS. Standard deviations were calculated from two different measurement series using independently purified CgCM preparations with the same CgDS stock that was used for crystallization. We noted that the apparent activation factors were up to twofold lower with other CgDS batches, possibly depending on varying degrees of intrinsic Trp occupancy (see below).

[b] Data from Sasso et al. *(32)*

We noted that the CgCM activity of the CgCM-CgDS complex is very sensitive to a multitude of variables including the absolute concentrations of chorismate, CgCM, and CgDS. For instance, the specific activity of CM increases with higher protein concentration, even when preserving the ratio of CM:DS. We have also observed that at 50 nM CgCM, the CM activity was linearly dependent on the concentration of its complex partner and could not be saturated in the experimentally accessible CgDS concentration range of 1-4 μM. This suggests that the $K_{d,\,app}$ for CgCM-CgDS complex dissociation exceeds 4 μM under our assay conditions.

Allosteric regulation of the CgCM-CgDS complex by Phe, Tyr, and Trp

To investigate feedback regulation at the central branch point in the shikimate pathway of *C. glutamicum,* the effect of aromatic amino acids on the catalytic efficiency of CM in the CgCM-CgDS complex was studied. Additions of single aromatic amino acids as well as combinations thereof were tested to elucidate potential synergistic effects. The kinetic assays were carried out with native CgCM and His_6-tagged CgDS, as it was shown previously that the correspondingly tagged homologous MtDS essentially retained the regulatory feedback properties of native MtDS *(36)*.

Given the experimental difficulties for reaching saturation, we aimed to derive physiologically meaningful information by contemplating concentrations of enzymes and effector molecules that approximate the conditions in the producer organism. From literature data, we estimated the concentrations of DS for the three organisms *M. tuberculosis* H37Rv, *Mycobacterium bovis* BCG, and *C. glutamicum* ATCC 13032, to be approximately 3 μM *(73, 74)*. For CM, the only reliably established concentration was 300 nM for *M. bovis (73)*. The chorismate concentration was estimated to be in the 40-70 μM range for *C. glutamicum (74, 75)*. Aromatic amino acid concentrations *in vivo* have been reported for *E. coli* to be 18 μM Phe, 29 μM Tyr, and 12 μM Trp *(76)*. As a compromise between experimentally accessible and naturally occurring concentrations, we used 1 μM CgDS, 100 nM CgCM, 100 μM chorismate, and 25 μM of each aromatic amino acid effector for the kinetic studies on the regulation of the CgCM-CgDS complex. Figure 3 illustrates the strong activation of CgCM activity through CgDS. Both Phe and Tyr reduce the activity of CgCM-CgDS (with Phe having a much stronger inhibitory effect). When combined, the inhibition of the CM activity by Phe and Tyr is synergistically enhanced. In contrast, Trp has a pronounced activating effect on the CM activity of CgCM-CgDS.

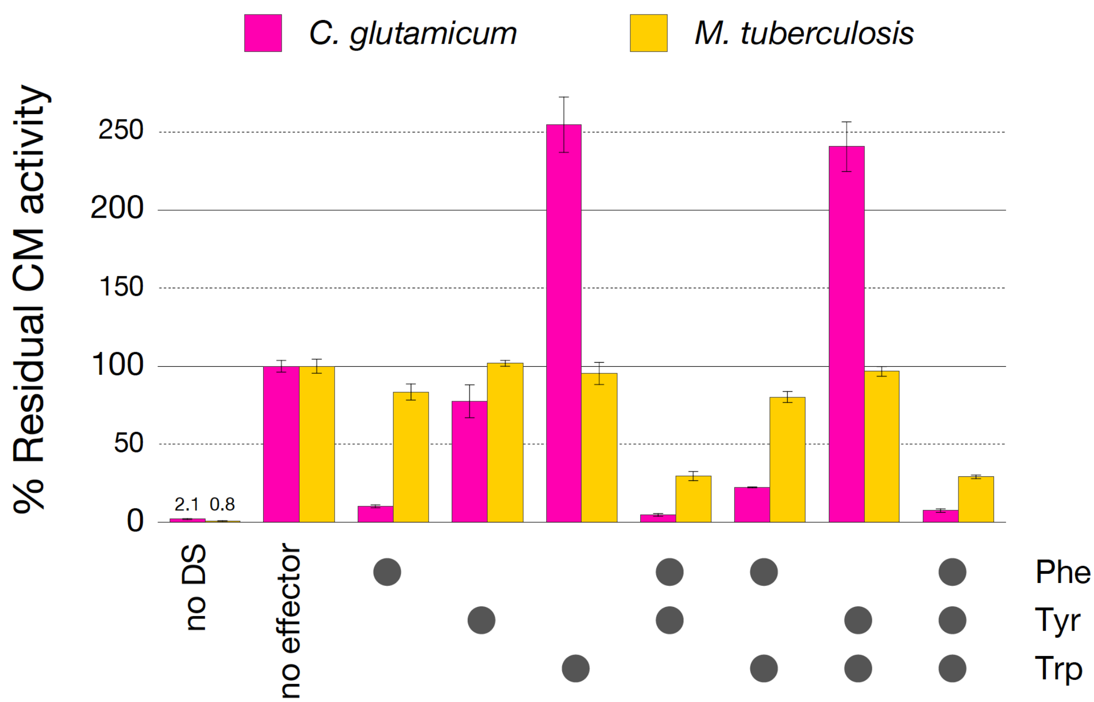

Figure 3. Allosteric regulation of CM-DS complexes from *C. glutamicum* and *M. tuberculosis*. The modulation of CM activity by Phe, Tyr, or Trp addition to the CM-DS complex (at 25 μM of each effector) is indicated relative to the activity in the absence of the effector (defined as 100%). Left columns (pink) represent CgCM-CgDS measurements, columns to the right (yellow) plot the data for the MtCM-MtDS system published previously *(36)*. For comparison, CM activity in the absence of a DS (and effectors) is shown on the left. Initial velocities were monitored at 30°C using 100 µM and 23 µM chorismate for CgDS-CgCM and MtDS-MtCM, respectively. Specific initial velocities (v_0/[CM]) of chorismate consumption without effectors were 1.55 ± 0.06 s^{-1} (100 nM CgCM; 1000 nM CgDS) and 4.0 ± 0.2 s^{-1} (30 nM MtCM; 300 nM MtDS). Error bars on the *C. glutamicum* data reflect standard deviations of at least four separate

measurements (using 2 independently purified batches of the CM). Whereas the absolute values in experiments with an independent, presumably compromised CgDS isolation differed by about twofold, the relative effects of Phe, Tyr, and Trp on CM activity of the respective complexes were approximately the same. All values are corrected for the spontaneous background reaction.

The general pattern of CgCM feedback inhibition is qualitatively similar to the one observed for the MtCM-MtDS complex, with Phe being a stronger inhibitor than Tyr *(35, 36)*. However, these inhibitory effects are consistently more pronounced for the enzymes from *C. glutamicum* at the applied near- physiological concentrations (Fig. 3). For instance, the residual CM activity of the CgCM-CgDS complex is reduced to a mere 10% by 25 μM Phe compared to 83% remaining activity for MtCM-MtDS. Also, synergistic inhibition by 25 μM each of Phe and Tyr reduces the CM activity to 5% for CgCM-CgDS, which is almost as low as the activity of CgCM on its own (2% of the value for CgCM-CgDS, under the experimental conditions given in Fig. 3). The corresponding values for the MtCM-MtDS system were 30% *(36)* and 0.8% (this work), respectively. The most prominent difference to the *M. tuberculosis* enzymes is that the addition of Trp increases the CM activity of the CgCM-CgDS complex by a factor of 2.5 (Fig. 3), whereas Trp had no effect on MtCM-MtDS at the same effector concentrations and enzyme ratios (Cg 100:1000 nM vs. Mt 30:300 nM, for CM:DS ratios, respectively). The activating effect by Trp is in accordance with observations from early investigations of CgCM *(77)*. Trp activation can (partially) offset inhibitory effects by the other amino acids (Fig. 3). In combination with Tyr, the activation by Trp is so prominent that the weak inhibition by Tyr alone is completely mitigated, resulting in net activation (to 240%) relative to the CM activity of the CgCM-CgDS complex.

Crystallographic analysis

To elucidate the molecular details of CgCM activation, we determined the crystal structures of CgCM, CgDS, and the CgCM-CgDS complex. The apo structure of CgCM was solved to 1.1 Å and refined to final R/R_{free}-factors of 0.17/0.22. For CgDS, data were collected for crystals with and without Trp soaked in (to 2.6 Å and 2.5 Å resolution, respectively, with R/R_{free}-factors of 0.25/0.28 and 0.24/0.25). The structure of the CgCM-CgDS complex was solved to a resolution of 2.2 Å (R/R_{free}=0.25/0.30), with a transition state analog (TSA in Fig. 1) bound in the active site of CgCM. For details on data collection and refinement statistics, see Table 1.

Crystal structure of CgCM

CgCM exhibits the typical structure of AroQ_{δ} subclass CMs, consisting of a homodimer with three α-helices making up each protomer (Fig. 4a). The crystal structure contains one protomer per asymmetric unit. There are two active sites per homodimer, positioned at the protomer interfaces. The N- and C-termini of CgCM are disordered, and part of the loop connecting helices H1 and H2 close to the active site (residues 43-45; Fig. 4a) is characterized by weaker electron density and somewhat increased *B*-factors, despite interactions with a symmetry-related molecule in the crystal (Fig. S1).

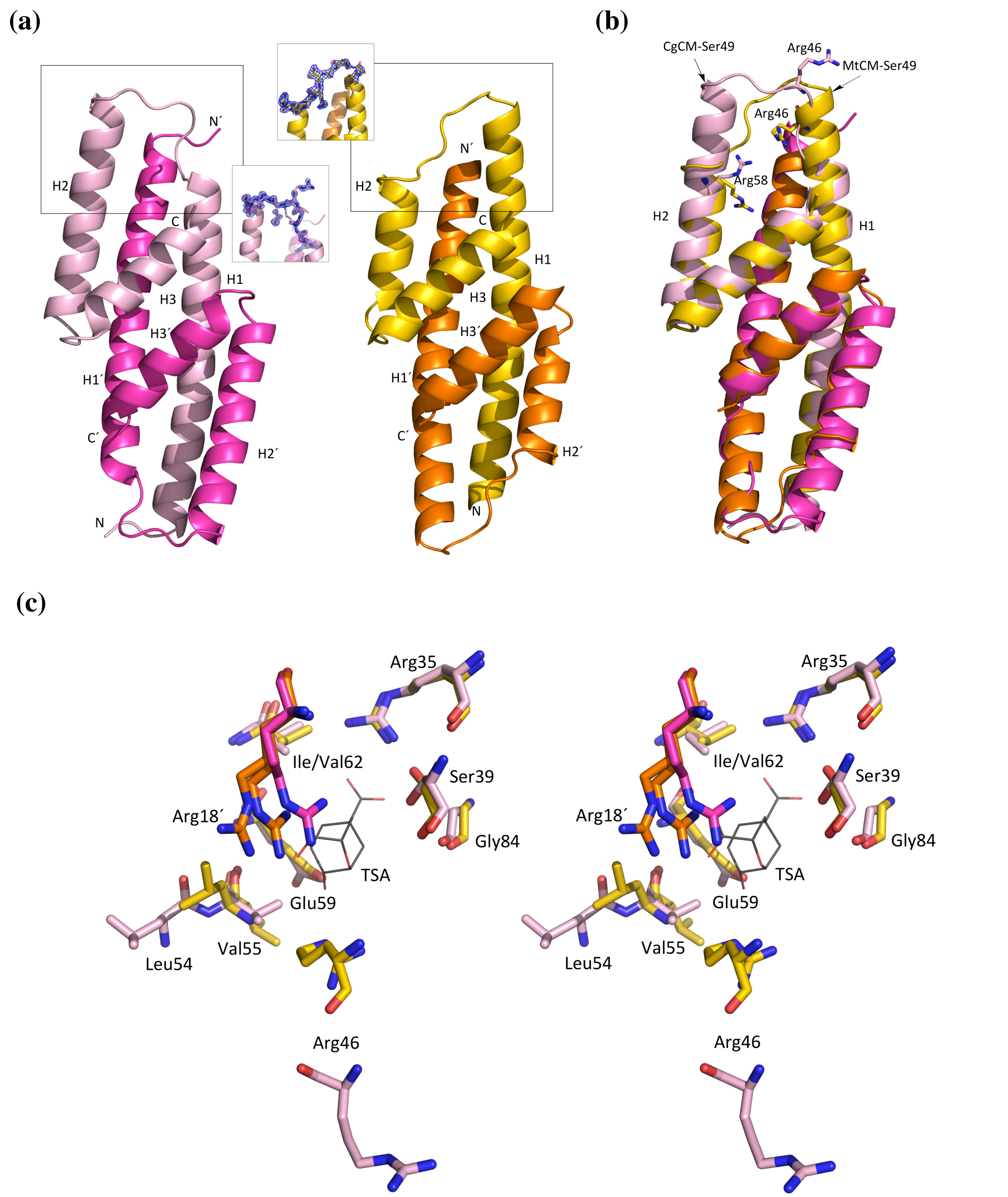

Figure 4. Structure of apo CgCM and comparison with apo MtCM. (a) CgCM (PDB ID: 5HUB, this work; pink) and MtCM (PDB ID: 2QBV; orange/yellow *(78)*) in their non-activated dimeric forms. The helices of the CgCM protomers are labeled as H1/H1' (residues 11-42), H2/H2' (residues 50-70) and H3/H3' (residues 74-85). The

boxed area shows a close-up view of the loop connecting H1 and H2, illustrating the electron density (blue mesh) of residues shown as sticks ($2mF_o - DF_c$ map, contoured at 1.5 σ). (b) Superimposition of the CgCM and MtCM enzymes, highlighting the unwound and extended helical segments, and the resulting differences in location and conformation of Arg46 and Arg58. (c) Superimposition of CgCM and MtCM active sites in the 'standard orientation' of Fig. 2c (TSA is superimposed from PDB ID: 2W1A *(32)* for comparison, drawn in thin lines; stereo image). Arg18´ is labeled with a prime and colored in a darker shade to show that this residue originates from the other protomer of the dimeric CM.

Structural comparison of CgCM with MtCM

Whereas the overall structures of CgCM (PDB ID: 5HUB, 1.1 Å resolution; this work) and MtCM (PDB ID: 2QBV *(78)*, 2.0 Å resolution, and PDB ID: 2VKL *(32)*, 1.65 Å resolution) are similar, the structures show clear differences close to the active site (Fig. 4). Many of these differences are probably not biologically relevant, however, due to extensive crystal contacts, which are different for the two structures (Fig. S1) (whereas CgCM crystallized in space group $C2$, MtCM crystallized in space group $P4_32_12$). In CgCM, helix H1 is shorter by two turns, whereas helix H2 is elongated by two turns. This has implications for the connecting loop, which has a different orientation in the two structures (Fig. 4a and b), and, consequently, for the positioning of catalytically important residues (Fig. 2b and Fig. 4b and c). In particular, the side chain of Arg46, the residue assumed to play the most crucial role in catalysis by stabilizing the developing partial negative charge in the transition state (Fig. 1 and Fig. 2b and c) *(79-81)*, is positioned far away from the active site in CgCM (Fig. 4b and c). In contrast, in MtCM, the guanidinium group of the corresponding Arg46 is less displaced relative to the catalytically productive conformation assumed in the activated enzyme.

The main conclusion from the comparison of the apo CM structures is that the H1-H2 loops and the adjacent active site region appears to be malleable and easily adapt to interact with other protein surfaces. This flexible nature is also reflected by the increased *B*-factors in this region, not only for CgCM, but also for both available free MtCM structures (PDB ID: 2QBV *(78)* and PDB ID: 2VKL *(32)*).

Crystal structure of CgDS

As observed for MtDS structures *(32-34, 36, 65, 82, 83)*, CgDS forms a homotetramer (Fig. 5). Each protomer consists of a central catalytic TIM barrel, which contains the DS active site featuring a Mn^{2+} ion and a PEP substrate molecule. The TIM barrel is decorated with small additional domains at the dimerization and tetramerization interfaces, like in MtDS *(32-34, 36, 65, 82, 83)* (Fig. 5). The N-terminus is oriented towards the dimerization interface, which is known to contain the Phe-binding site in MtDS *(33, 34, 36, 82)*. However, in CgDS the N-terminus is not well defined by electron density until residue 25; therefore, a tight interaction, as seen between the N-terminal β-strands of MtDS *(36, 65)*, is not observable in CgDS. Close inspection of the tetramerization interface revealed electron density that can be attributed to Trp (Fig. S2). The density is observed in the same pocket where Trp is known to bind in the MtDS structures *(33, 34, 36, 82)*.

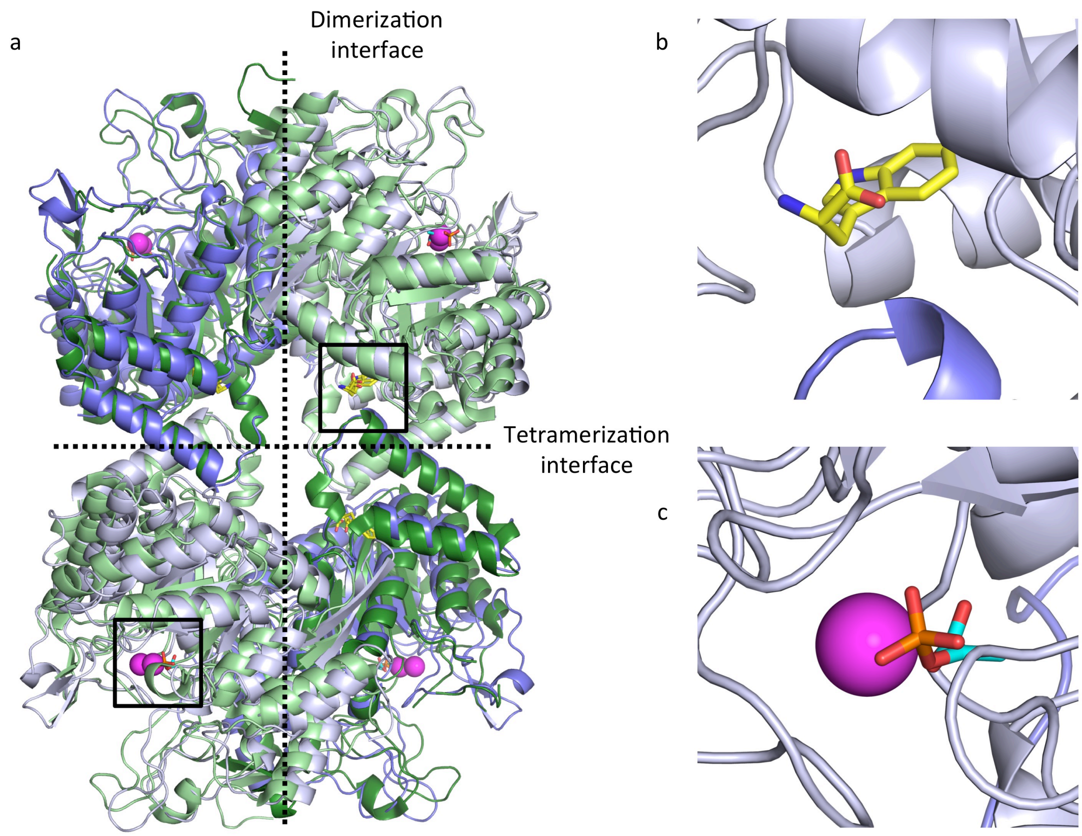

Figure 5. **Crystal structure of CgDS and comparison with MtDS.** (a) Cartoon image showing the superimposition of CgDS (PDB: 5HUC**,** this work; violet/grey) and MtDS homotetramer (PDB: **3**NUE *(82)*; green. The dashed lines illustrate the dimerization and tetramerization interfaces of the DS tetramer, and the squares indicate the location of the DS active site and the Trp binding site in one of the DS protomers. (b) Close-up view of the CgDS Trp binding site, with Trp shown as yellow sticks. (c) Close-up view of the CgDS active site, with a Mn^{2+} ion (magenta sphere) and bound substrate (PEP, sticks with carbons in cyan).

Crystal structure of the non-covalent CgCM-CgDS complex

The overall structure of the CgCM-CgDS complex shows a tetrameric assembly of CgDS, decorated with two CgCM dimers at opposing sides at the periphery to form a heterooctamer, analogous to its *M. tuberculosis* counterpart *(32)* (Fig. 6a and b). In contrast to the uncomplexed CM apo structures, the conformations of the CgCM-CgDS and MtCM-MtDS complexes with TSA are very similar (Fig. 6b) [backbone r.m.s.d. = 0.37±0.03 Å between CgCM-CgDS (PDB ID: 5HUD, this work) and MtCM-MtDS (PDB ID: 2W1A *(32)*)]. The similarity extends to the individual subunits (r.m.s.d. = 0.41±0.02 Å for DSs and 0.43±0.03 Å for CMs).

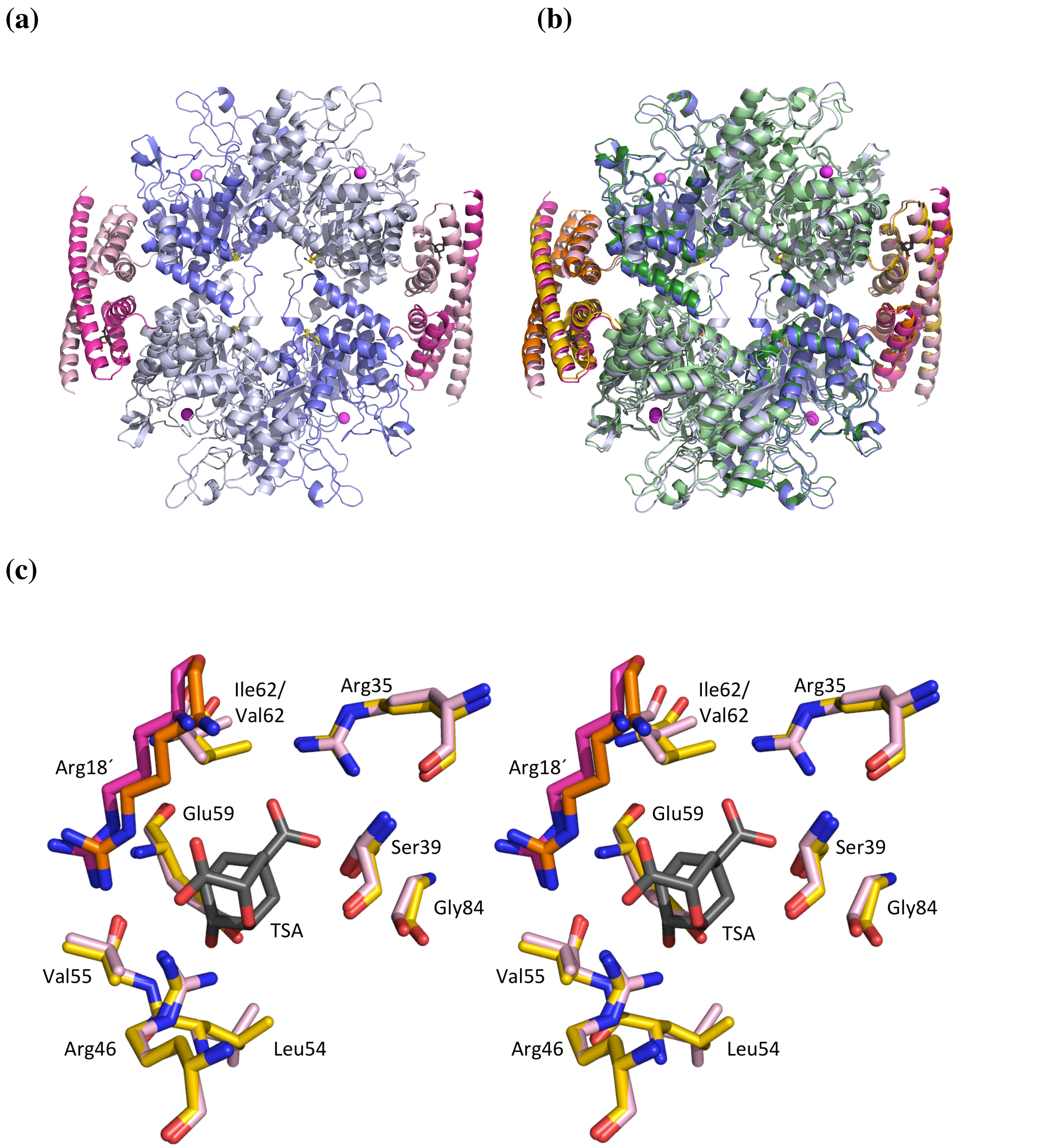

Figure 6. **Structure of the CgCM-CgDS complex and comparison with MtCM-MtDS.** (a) Cartoon image of the CgCM-CgDS heterooctameric complex. CgCM is colored in pink and CgDS in shades of violet to emphasize individual subunits. Mn^{2+} ions are shown as magenta spheres. (b) Superimposition of the CgCM-CgDS (violet) and MtCM-MtDS (PDB: 2W1A *(32)*; green) complexes (overview). (c) Stereo image of the

activated CM active sites, with CgCM-CgDS (PDB ID: 5HUD, this work; pink) and MtCM-MtDS (PDB ID: 2W1A *(32)*; yellow/orange) superimposed. Arg18´ is labeled with a prime and colored in a darker shade to show that this residue originates from the other protomer of the dimeric CM.

Also the catalytically relevant residues (Arg35, Ser39, Arg46, Val55, Glu59, and Arg18', where the prime refers to the other protomer in the CM homodimer) in the respective DS complexes superimpose well between MtCM and CgCM (Fig. 6c). All of these residues adopt their active conformations, providing a structural explanation for the apparent 180-fold rate acceleration measured for CgCM (Table 2). The biggest conformational change is observed for the catalytic residue Arg46 (a 13 Å relocation of $C\zeta$), which flips into the active site to interact with TSA through its ether oxygen and one of its two carboxylates. The changes within CgCM coincide with an observable extension of helix H1 and a shortening of helix H2 upon interaction with CgDS.

When comparing the CgDS-CgCM interface with the corresponding CgDS apo structure, we observe three major structural adaptations of CgDS: (i) formation of a salt bridge between Arg223 and Glu468, avoiding clashes with CM residues 59-60 and 63; (ii) reorientation of Gln402 to H-bond with the backbone NH of Gly90 at the C-terminus of CgCM; (iii) reorientation of Asn472 affecting Arg409, which adopts a dual conformation, clutching the C-terminal carboxylate of CgCM from two sides. In addition, Glu461 slightly alters its conformation to avoid interference with CgCM residue His56. All of these conformational changes favor the interaction with CgCM, promoting its catalytically competent conformation. In particular, the CM C-terminus is reshaped to constructively interact with residues close to the CM active site (*e.g.*, Leu89 interacts with Leu54, less than 4 Å apart). Of the three described adaptations (i-iii), the first two are similar to those observed for the *M. tuberculosis* enzymes *(36)*. The structural adaptations (iii) are not directly comparable because the C-termini of the two uncomplexed apo CMs adopt widely different conformations that are also affected by crystal contacts.

Somewhat unexpected was the observation of additional helical fragments at the N-termini of two CgDS molecules (despite the fact that the N-terminus of CgDS, which is fused to a His_6 purification tag, is predicted to be flexible). These fragments were modeled as residues 7-17 of CgDS. They are located in solvent channels of the crystal and unlikely to affect complex formation or CgCM activation. As for the CgDS structure, we observed the presence of Trp in the CgCM-CgDS complex (see below), even though no Trp was added at any time for those structural studies.

Possible origin of CgCM activation by Trp

All CgDS crystal structures, including the CgCM-CgDS complex, were found to contain Trp to different extents. As this compound was not added at any time during purification and crystallization, its most likely origin is co-purification from the cell lysate. Visual inspection of the electron density revealed that both apo CgDS and the CgCM-CgDS complex show significant occupancy of Trp in its binding pocket that was clearly increased upon soaking of CgDS crystals with Trp (see Fig. S2). This is also reflected by the *B*-factors of the Trp-ligand compared to interacting protein residues, which are essentially identical for the structure of the CgDS/Trp soak, whereas they are approximately 20 Å^2 higher (Trp compared to protein) for the CgCM-CgDS and apo CgDS structures (note that the occupancy was modeled at 100% for all three structures). The two CgDS structures (and the DS part of the heterooctameric enzyme complex; Fig. S3) show no significant structural differences in the Trp binding sites. A close examination of the previously published structures of MtDS without Trp (PDB ID: 2W1A *(32)*, 3NV8 *(82)*, and 2B7O *(65)*) suggests that it is unlikely that there are any trace amounts of Trp present in those structures, as there is no positive difference electron density. In one of the protomers (PDB ID: 2B7O *(65)*), the Gln239 side chain even points directly into the empty Trp binding pocket, where it would clash with Trp if bound there.

The Trp binding site is located at the center of the CgDS tetramer, close to both dimerization and tetramerization interfaces, and at the same position as in MtDS (Fig. 7). This effector buries 291 Å^2 and 58 Å^2 from the involved two subunits (for comparison, 307 Å^2 and 60 Å^2 are buried in MtDS) (Table S1). The hydrogen bonding pattern between Trp and CgDS is also analogous to that observed in the MtDS–Trp structure (PDB ID: 3NUE *(82)*) and in fully inhibited MtDS (PDB ID: 5CKV *(36)*) (compare Fig. 7a and c). As shown in Figure 7a, the indole NH group of Trp forms a hydrogen bond to the backbone carbonyl group of Ala202 of CgDS, the Trp carboxylate to the side chain of Lys133, and the Trp amino group to the backbone carbonyl groups of Ala250 and Ser247. The hydroxyl group of Ser247, in turn, forms a hydrogen bond across the tetramer interface to the backbone carbonyl group of Cys241 (Fig. 7a and b). In MtDS, the analogous interaction across the tetramer interface is mediated through Asn237, which provides an H-bond to the carbonyl oxygen of the homologous Cys231 (in one of the MtDS subunits, Asn237 adopts alternative conformations, one H-bonding to Cys231 and the other to the adjacent Gly232 residue) (Fig. 7c and d). Another difference between CgDS and MtDS is the involvement of Leu207 in a prominent van der Waals interaction with Trp in CgDS, a role played by Val197 in MtDS.

(a)

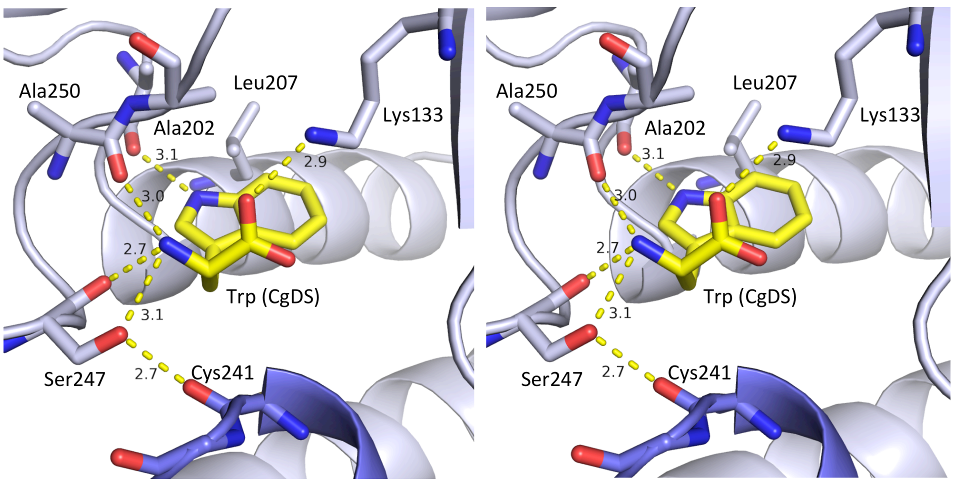

(b)

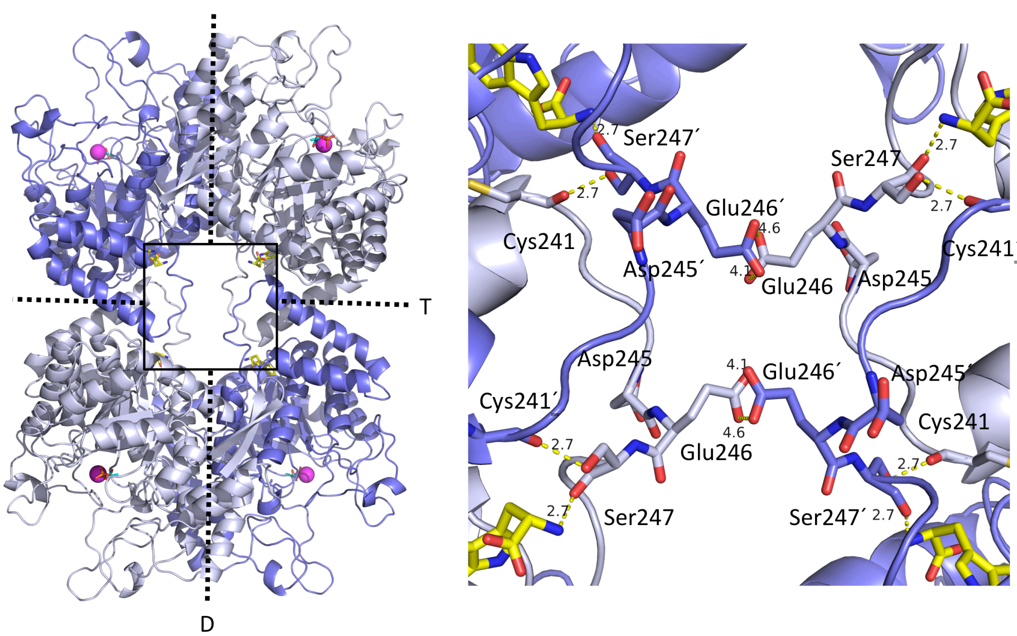

(c)

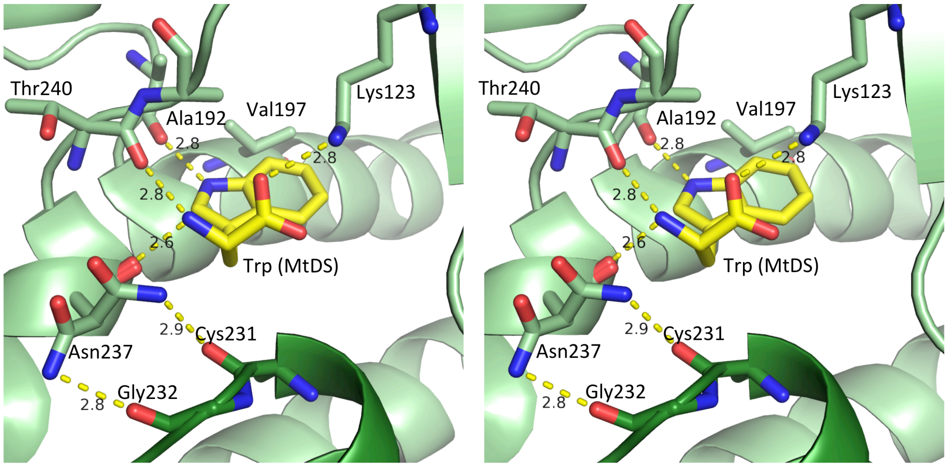

(d)

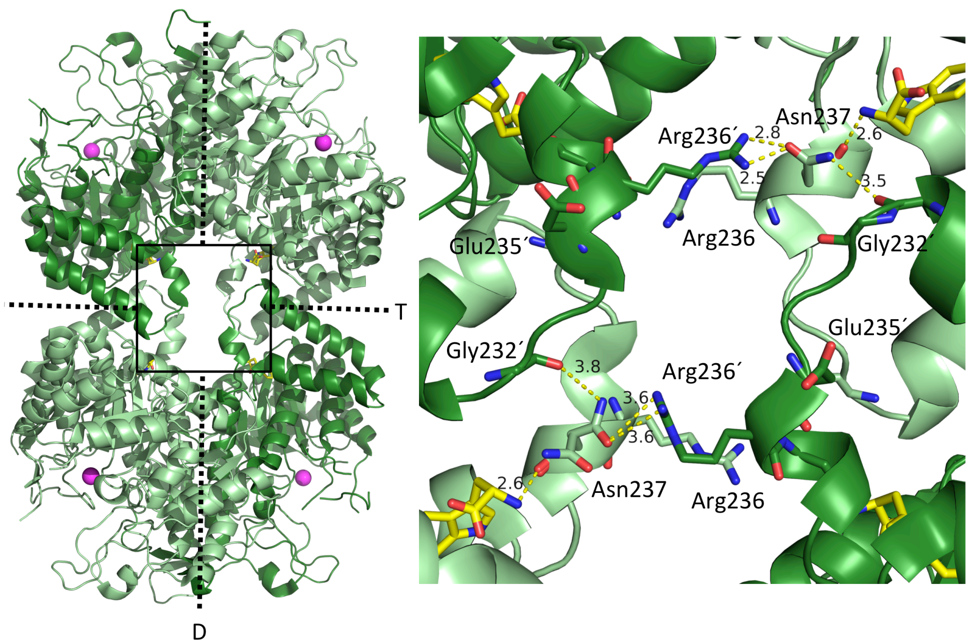

Figure 7. Structure of DS in complex with the allosteric regulator Trp. (a) Stereo image of CgDS Trp binding pocket (Trp, yellow sticks), and interactions across tetramerization interface. (b) CgDS homotetramer (PDB: 5HUE, this work, violet/grey). Mn^{2+} ions (magenta spheres) and PEP (sticks with carbons in cyan) indicate DS active sites. Trp (yellow sticks) binds at the tetramerization interface (indicated by T) and in close proximity to the dimerization interface (indicated by D). Box: close-up view of the

CgDS tetramer core, displaying interactions across the dimer interface. (c) Stereo image of the MtDS Trp binding pocket and interactions across the tetramerization interface. (d) MtDS homotetramer (PDB: 3NUE, green/light green *(82)*), with Mn^{2+} ions in magenta. Trp (yellow sticks) binds to equivalent locations compared to CgDS. Box: close-up view of the MtDS dimer interface at the MtDS tetramer core. Prime superscripts were used to differentiate between protomers in the DS tetramer.

Additional unique features distinguishing CgDS from MtDS are observed at the dimerization interfaces (Fig. 7b and d). Whereas in CgDS, a number of acidic residues accumulate at the center of the homotetramer (four copies each of Glu246 and, at some distance, of Asp245), in MtDS the homolog of Glu246 is an arginine residue (Arg236). This basic residue extends its alkyl guanidinium side chain across the dimerization interface and interacts with Asn237 from a different DS protomer, a residue that is in the direct interaction sphere of Trp (Fig. 7c and d). The MtDS homotetramer in complex with Trp (PDB ID: 3NUE *(82)*) is clearly more structured at its core compared to its CgDS equivalent (PDB ID: 5HUE, this work), which exhibits very poor electron density for the central Glu246 carboxylate groups. Nevertheless, the distances across the DS core are essentially identical between the two structures (compare Figs. 7b and d).

Previously, we reported a slight shift in the relative alignment of MtDS subunits (rotation by 1-2°) in the MtCM-MtDS complex as a result of the binding of the feedback inhibitors Phe and Tyr (comparison of PDB ID: 2W1A *(32)* with 5CKX *(36)*) *(36)*. This realignment is hardly visible at the interface with CM, but more pronounced towards the DS dimer interface. MtDS in complex with Trp exhibits a realignment of similar magnitude, but in the opposite direction (comparison of PDB ID: 2W1A *(32)* with 3NUE *(82)*), which brings the DS subunits closer together at the tetramer interface (not previously described). In this work, we calculated relative subunit realignments slightly differently, comparing helix axes at the DS tetramer interface. The results show similar trends for the comparisons above, but give slightly larger values (3-4°). CgDS in complex with Trp (PDB ID: 5HUE; this work) adopts a similar conformation as the MtDS-Trp complex (PDB ID: 3NUE *(82)*). In comparison, apo MtDS (from PDB ID: 3NV8 *(82)* rather than PDB ID: 2B7O *(65)*, which contains a PEG molecule in the Phe-binding site) is more "closed" towards the periphery, where CM would dock (Fig. S4). The relative alignment of CgDS subunits in the Trp complex hence lies between that of the DS apo form (derived from comparisons with the available MtDS structure PDB ID: 3NV8 *(82)*) and the CgDS complex with CgCM (PDB ID: 5HUD; this work) (Fig. S4), which may suggest that Trp binding can prime CgDS for productive complex formation with CgCM and thus promote CgCM activation.

DISCUSSION

CgCM is activated by CgDS

The kinetic and structural data presented here show that CgCM activity can be boosted by CgDS in analogy to what has been observed for the corresponding enzymes from *M. tuberculosis*. Even though the apparent k_{cat}/K_m for CgCM and CgCM-CgDS under the assay conditions is lower by an order of magnitude compared to MtCM and the MtCM-MtDS complex, respectively, the factor of activation afforded by DS is in a similar range (180-fold for CgCM[1] compared to 140-fold for MtCM). Thus, our results directly contradict the findings by Li *et al*. *(54)*, who did not observe activation of CgCM by CgDS. We suspect that the activating effect by CgDS could have been hard to detect because the CgCM activity enhancement is very sensitive to a multitude of factors in addition to the CM:DS ratio, such as the absolute substrate and enzyme concentrations or the formats of the enzymes used. In this context, it must be noted that the His-tagged CgCM format used in the study by Li *et al*. *(54)* includes up to 31 additional amino acids at the N-terminus with respect to our untagged, and —compared to the Cgl0853 annotation— shorter CgCM. Even though the N-terminus of CgCM does not seem to be in close proximity of the CgDS surface *(36)*, a 30% elongated CM version might show altered interaction behavior.

Activation of CgCM by CgDS was already reported much earlier, however. At that time, it was still assumed that the CM was split into two parts, one of which would be found fused to DS, forming a *bona fide* bifunctional enzyme *(52, 53)* The studies by

[1]Since Trp was found to additionally increase CM activity in the CgCM-CgDS complex, the extent of CgCM activation by CgDS alone may be somewhat overestimated due to possibly stoichiometrically bound residual Trp in CgCM-CgDS preparations. Any resulting basal Trp level (at most 0.5-1 µM) in the assays, however, is still much lower than the 25 µM effector used for the kinetic studies.

Shiio and Sugimoto *(52)*, and Sugimoto and Shiio *(53)* were carried out with the organism *Brevibacterium flavum*, which was only later reclassified as *C. glutamicum (51)*, thus suggesting that they were actually characterizing the CgCM-CgDS protein complex. Furthermore, we have shown previously that CgCM can be heterologously activated with MtDS by more than an order of magnitude *(32)*.

Structural similarity to CM-DS complex in *M. tuberculosis*

Overall, the crystal structures of CgCM, CgDS, and the CgCM-CgDS complex are very similar to those of their *M. tuberculosis* homologs. The clear similarities between the CgCM-CgDS and MtCM-MtDS complexes extend to the CM active site and imply that the activation of CM occurs by the same mechanism through optimizing the positioning of active site residues (*e.g.,* Arg18', Arg46, and Val55). The largest structural differences are found when comparing free apo CgCM with the corresponding MtCM. As detailed in the *Results* section, those dissimilarities are likely caused by crystal contacts, but reflect the malleability of the H1-H2 linker region. This property may also allow the active conformation to be adopted relatively easily upon binding to CgDS.

Regulation by inter-enzyme allostery – Similarities and differences

As for the MtCM-MtDS complex, association of CgCM with its complex partner enables allosteric regulation by inter-enzyme allostery *(36)*. It was demonstrated for the *M. tuberculosis* system that binding of the feedback inhibitors Phe and Tyr to their allosteric sites on DS dissociates the complex with CM, essentially resulting in shutting off CM activity. We now report that the regulatory effects of the aromatic acids are even more pronounced in *C. glutamicum* than in *M. tuberculosis*. This may partly be connected with the much higher $K_{d,app}$ of CgCM-CgDS (> 4 μM) compared to the MtCM-MtDS complex (≈ 140 nM *(32)*). At the enzyme concentrations below $K_{d,app}$, as employed in the kinetic measurements with CgCM (100 nM) and CgDS (1000 nM), a greater magnitude of CM activity modulation would thus have been apparent compared to the data collected at the saturating enzyme concentrations (above the $K_{d,app}$) for the MtCM-MtDS system. The magnitude of the regulation is, depending on the system studied, also quite sensitive to the effector concentrations used in the assay. In fact, previous investigations on CM-DS complex inhibition at 100-200 μM of each amino acid *(32, 35, 53, 84)* gave significantly different results than the 25 μM used in this work, a concentration we estimate to better reflect conditions encountered inside a bacterial cell *(36, 76)*.

The structural and kinetic data presented here extend the recently discovered novel paradigm for regulation of the shikimate pathway *(35, 36)* to another member of the class of *Actinobacteria*. Activation of CM by DS, and inter-enzyme allosteric inhibition by Phe and Tyr represent clear similarities between *C. glutamicum* and *M. tuberculosis*. However, there are also differences, in particular the observed activating effect of Trp on CM catalysis for the CgCM-CgDS complex. Whereas activation by Trp has also been reported for a CM from *B. flavum* *(52, 53, 74)*, enhanced CM activity by Trp has not been described for the previously characterized MtCM-MtDS system.

Trp enhances CgCM activation by CgDS

An activating effect of Trp on chorismate mutases is known to operate in yeast (*Saccharomyces cerevisiae) (85, 86)* and plants *(87, 88)*, and this cross-pathway activation appears to be a general mechanism nature has developed to fine-tune the flux through the shikimate pathway. – But how does Trp enable the substantial activation of CgCM? In analogy to the *M. tuberculosis* system *(33, 35, 36, 38)*, inter-enzyme allosteric regulation of CgCM may result from small realignments of the CgDS subunits or alternatively from differences in dynamics, caused by the binding of allosteric effectors. These changes need to be transmitted approximately 30 Å from the allosteric binding sites at the oligomerization interfaces of CgDS to its interface with CgCM. Certainly, optimal geometric and electronic complementarity at this interface between the CgDS homotetramer and the CgCM dimer is crucial for productive interaction and hence CM activation, but also the stability of the entire complex is likely to play a role.

Model of feedback regulation of the shikimate pathway in *C. glutamicum*

Trp is positioned at four locations at the DS tetramerization interface, each linking two DS subunits of the homotetramer (Fig. 7b). Since the tetramerization interface is characterized by a smaller interaction surface compared to the dimerization interface (855 versus 1069 Å^2 without Trp), Trp could provide an additional surface to hold the tetramer together, potentially aiding complex formation with CM. Optimal arrangement of DS subunits is expected to promote binding of the CM homodimers and hence boost their catalytic activity. The realignment of DS subunits upon Trp binding is likely to contribute positively in this respect, as it opens up the CM docking site at its periphery (Fig. S4). In contrast, the binding of the feedback inhibitor Phe, which induces a register shift at the N-termini of the DS and tightly clamps Trp3 from two sides, as discussed previously *(36)*, may lock the DS in an unfavorable conformation with respect to CM binding and activation. This tight "inter-locking" interaction with DS by Phe may dwarf the activating effect of Trp (Fig. 3), essentially shutting down CM activity (Fig. 8).

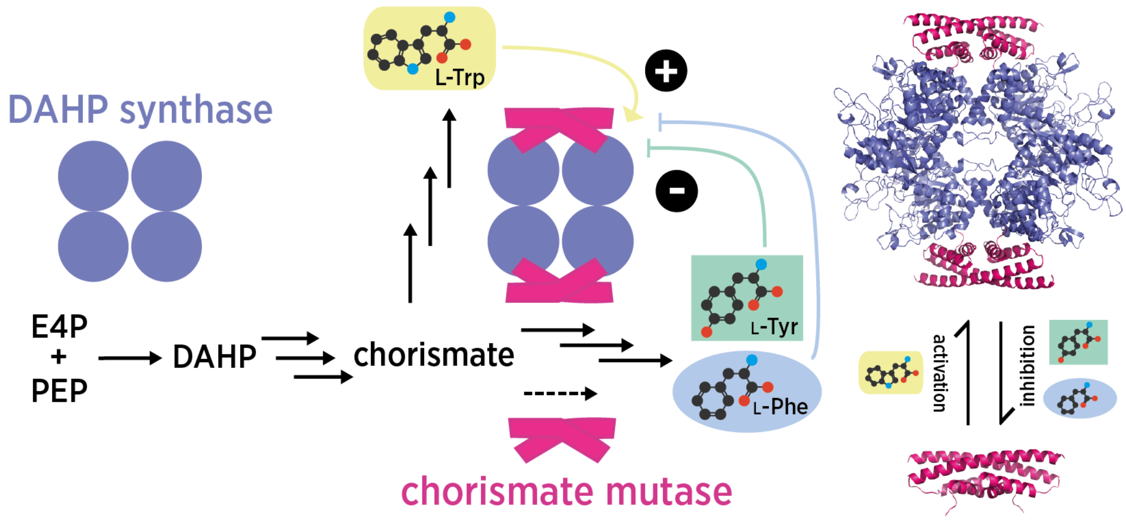

Figure 8. Proposed mechanism of CgCM regulation. From left to right: The first enzyme of the shikimate pathway, DAHP synthase, catalyzes the conversion of D-erythrose-4-phosphate (E4P) and phosphoenolpyruvate (PEP) to 3-deoxy-D-arabino-heptulosonate-7-phosphate (DAHP). CM is positioned at the branch point of the shikimate pathway, towards synthesis of L-Phe and L-Tyr (and away from L-Trp). Its naturally poor activity is boosted by complex formation with DAHP synthase by 180-fold. L-Trp serves as allosteric activator, by promoting complex formation of CgCM with CgDS. It does so by binding to CgDS at the center of the DS tetramer, approximately 30 Å from the CM-docking site, stabilizing the tetrameric DS at close-to-optimal geometry for binding of CM. When the feedback inhibitors L-Phe and L-Tyr (with or without L-Trp) bind to their allosteric sites within the DS, the DS N-termini are "clamped" together. This leads to a conformational change at the DS binding interface and dissociation of CgCM from the CM-DS complex, and ultimately to downregulation of CM catalysis to its stand-alone mediocre activity.

Why is CgCM regulation different from MtCM?

Whereas the regulation of CgCM and MtCM activity is generally similar, a key difference is the activating effect of Trp on CM catalysis in the CgCM-CgDS complex, which has not been observed for MtCM. Possible causes of this difference could be a higher affinity of Trp to CgDS, a more optimal geometry or electronic complementarity of CgDS for CgCM compared to MtCM-MtDS, or differences in the dynamics of the two systems. The fact that traces of Trp are observed in all CgDS structures (but not in MtDS), despite its absence during purification and crystallization, suggests that Trp may indeed be retained more strongly by CgDS[2]. Still, the Trp binding sites of CgDS and MtDS are rather similar (Fig. 7a and c), and do not suggest significant differences in binding affinities. There are two amino acid differences in CgDS compared to MtDS that could affect Trp binding, namely Ser247 (MtDS: Asn237) and Leu207 (MtDS: Val197), but their interactions with the ligand and the buried surface areas are comparable (Table S1).

We do, however, observe significant differences between the two structures at the DS tetramer core, which could influence geometry and dynamics. In CgDS, a cluster of acidic residues (four copies each of Asp245 and Glu246) dominates the tetramer core, whereas MtDS exhibits a more balanced profile of acidic (Asp235) and basic (Arg236) residues, and its two DS halves are more tightly connected across the dimer interface by interactions between Arg236 and Asn237 from a neighboring protomer (compare Figs. 7b

[2]Note that we cannot exclude with certainty that the complex with Trp has been selected for due to preferential crystallization.

and d). The differential amino acid interactions in the interface region are likely to affect local conformations (note for instance the additional helical turns at the MtDS tetramer core; Fig. 7d) as well as the overall tetramer alignment and dynamics, with possible consequences for DS's ability to bind and activate CM. Electrostatic repulsion across the CgDS tetramer core (Fig. 7b) may facilitate opening of the DS tetramer at its periphery towards CM, explaining the strong activating effect of Trp in the CgCM-CgDS system, whereas in MtDS, the interactions between Arg236 and Asn237, and between the Arg236 side chains from different protomers (Fig. 7d) may limit the dynamics and hence the activation potential of Trp. Possibly, these dissimilarities lie at the heart of the observed differences in feedback activation. It cannot be ruled out, however, that the chosen experimental conditions, despite our best efforts, insufficiently model the biological environment, and that Trp has some potential to promote CM activity in the CM-DS complex in both systems. Cross-pathway activation by Trp would certainly make sense biologically, as it enables the bacteria to efficiently redirect the metabolic flow at the crucial shikimate pathway intermediate chorismate into other branches, as soon as the cellular needs for Trp are met.

PERSPECTIVES

The knowledge gained about the regulatory details of the shikimate pathway could be very useful for several reasons. *C. glutamicum* is an important bacterium for the biotechnological production of amino acids, nucleotides, and vitamins. In fact, metabolically engineered strains have been developed for the fermentation of L-glutamate, which has been utilized for more than 50 years as an industrial food additive *(89)*. Elucidation of the structure and function of key shikimate pathway enzymes are highly relevant for industrial innovations, as understanding of the natural feedback regulatory mechanisms can inform strategies to eliminate potential bottlenecks in large-scale biotechnological production. For instance, abolishing the feedback inhibition of DAHP synthase in *Saccharomyces cerevisiae* by mutagenesis resulted in a 200-fold increase in extracellular aromatic amino acid concentration *(90)*, and corresponding rationally designed enzyme variants immune to the natural feedback regulation may prove beneficial for *C. glutamicum* production strains, too. Furthermore, since the here described CM-DS regulation mechanism is confined to just some orders of the phylum *Actinobacteria*, which also includes pathogens responsible for diseases like tuberculosis and leprosy *(36)*, our insights into the molecular details of the regulation of a central biosynthetic pathway may facilitate the development of pathogen-specific drugs.

ASSOCIATED CONTENT

Supporting Information.

The following file is available free of charge: Crystal contacts in apo CgCM, comparison of electron density in CgDS Trp binding pockets, comparison of CgDS structures, structural comparison of CgDS with MtDS, and surface area of Trp interface in CgDS and MtDS (PDF).

AUTHOR INFORMATION

Corresponding Authors

*(P.K.) - Phone: +41 44 632 2908. E-mail: kast@org.chem.ethz.ch

*(U.K.) - Phone: +47-22 85 54 61. E-mail: ute.krengel@kjemi.uio.no.

Present Address

[†]D. Burschowsky, Leicester Institute of Structural and Chemical Biology, University of Leicester, Leicester, UK

Author Contributions

[§]These authors contributed equally to this work. P.K. and U.K. conceived the study; D.B., H.V.T., J.B.H, J.F.-K., and K.W.-R. performed the experiments, supervised by P.K. and U.K.; all authors analyzed the data; U.K. validated the crystal structures; and all authors contributed to writing the paper.

Funding Sources

This study was financed by funds from the University of Oslo (positions of HVT and JBH), the ETH Zurich, the Norwegian Research Council (grants no. 214037 and 216625), and the Swiss National Science Foundation (grants no. 31003A-116475, 31003A-135651, and 31003A-156453).

ACKNOWLEDGMENT

We wish to thank the ESRF for synchrotron beam time and user support.

ABBREVIATIONS

Bicine, N,N-bis(2-hydroxyethyl)glycine; CgCM, *Corynebacterium glutamicum* chorismate mutase encoded by Cgl0853; CgDS, *C. glutamicum* DAHP synthase encoded by Cgl2391; CM, chorismate mutase; Bis-Tris, (1,3-bis[tris(hydroxymethyl)methylamino]); DAHP, 3-deoxy-D-arabino-heptulosonate-7-phosphate; DS, DAHP synthase; E4P, D-erythrose-4-phosphate; HEPES, 4-(2-hydroxyethyl)piperazine-1-ethanesulfonic acid, *N*-(2-hydroxyethyl)piperazine-*N*'-(2-ethanesulfonic acid); IPTG, isopropyl β-D-1-thiogalactopyranoside; LC-MS, liquid chromatography–mass spectrometry; MES, 2-(*N*-morpholino)ethanesulfonic acid; MME, monomethyl ether; MR, molecular replacement; MtCM, *Mycobacterium tuberculosis* chorismate mutase encoded by Rv0948c; MtDS, *M. tuberculosis* DAHP synthase encoded by Rv2178c; PCR, polymerase chain reaction; PEG, polyethylene glycol; PEP, phosphoenolpyruvate; Phe (or F), L-phenylalanine; PMSF, phenylmethane sulfonyl fluoride or phenylmethylsulfonyl fluoride; r.m.s.d., root mean square difference/deviation; TCEP, (tris[2-carboxyethyl]phosphine hydrochloride); Tris, tris(hydroxymethyl)aminomethane; Trp (or W), L-tryptophan; TSA, transition state analog; Tyr (or Y), L-tyrosine

REFERENCES

(1) Jacob, F., and Monod, J. (1961) Genetic regulatory mechanisms in the synthesis of proteins, *J. Mol. Biol. 3*, 318-356.

(2) Perutz, M. F. (1989) Mechanisms of cooperativity and allosteric regulation in proteins, *Q. Rev. Biophys. 22*, 139-236.

(3) Jensen, R. B., and Shapiro, L. (2000) Proteins on the move: Dynamic protein localization in prokaryotes, *Trends Cell Biol. 10*, 483-488.

(4) Vogel, C., and Marcotte, E. M. (2012) Insights into the regulation of protein abundance from proteomic and transcriptomic analyses, *Nat. Rev. Genet. 13*, 227-232.

(5) Liu, H., Urbé, S., and Clague, M. J. (2012) Selective protein degradation in cell signalling, *Semin. Cell Dev. Biol. 23*, 509-514.

(6) Motlagh, H. N., Wrabl, J. O., Li, J., and Hilser, V. J. (2014) The ensemble nature of allostery, *Nature 508*, 331-339.

(7) Verdin, E., and Ott, M. (2015) 50 years of protein acetylation: From gene regulation to epigenetics, metabolism and beyond, *Nat. Rev. Mol. Cell Biol. 16*, 258-264.

(8) Humphrey, S. J., James, D. E., and Mann, M. (2015) Protein phosphorylation: A major switch mechanism for metabolic regulation, *Trends Endocrinol. Metab. 26*, 676-687.

(9) Berezovsky, I. N., Guarnera, E., Zheng, Z., Eisenhaber, B., and Eisenhaber, F. (2017) Protein function machinery: From basic structural units to modulation of activity, *Curr. Opin. Struct. Biol. 42*, 67-74.

(10) Monod, J., Changeux, J.-P., and Jacob, F. (1963) Allosteric proteins and cellular control systems, *J. Mol. Biol. 6*, 306-329.

(11) Monod, J., Wyman, J., and Changeux, J.-P. (1965) On nature of allosteric transitions: A plausible model, *J. Mol. Biol. 12*, 88-118.

(12) Cornish-Bowden, A. (2014) Understanding allosteric and cooperative interactions in enzymes, *FEBS J. 281*, 621-632.

(13) Herrmann, K. M., and Weaver, L. M. (1999) The shikimate pathway, *Annu. Rev. Plant Physiol. Plant Mol. Biol. 50*, 473-503.

(14) Tzin, V., and Galili, G. (2010) New insights into the shikimate and aromatic amino acids biosynthesis pathways in plants, *Molecular Plant 3*, 956-972.

(15) Maeda, H., and Dudareva, N. (2012) The shikimate pathway and aromatic amino acid biosynthesis in plants, *Annu. Rev. Plant Biol. 63*, 73-105.

(16) Light, S. H., and Anderson, W. F. (2013) The diversity of allosteric controls at the gateway to aromatic amino acid biosynthesis, *Protein Sci. 22*, 395-404.

(17) Wallace, B. J., and Pittard, J. (1967) Genetic and biochemical analysis of isoenzymes concerned in first reaction of aromatic biosynthesis in *Escherichia coli*, *J. Bacteriol. 93*, 237-244.

(18) Umbarger, H. E. (1978) Amino acid biosynthesis and its regulation, *Annu. Rev. Biochem. 47*, 532-606.

(19) Shumilin, I. A., Kretsinger, R. H., and Bauerle, R. H. (1999) Crystal structure of phenylalanine-regulated 3-deoxy-D-*arabino*-heptulosonate-7-phosphate synthase from *Escherichia coli*, *Structure 7*, 865-875.

(20) Bartlett, P. A., and Johnson, C. R. (1985) An inhibitor of chorismate mutase resembling the transition-state conformation, *J. Am. Chem. Soc. 107*, 7792-7793.

(21) Sogo, S. G., Widlanski, T. S., Hoare, J. H., Grimshaw, C. E., Berchtold, G. A., and Knowles, J. R. (1984) Stereochemistry of the rearrangement of chorismate to prephenate: Chorismate mutase involves a chair transition state, *J. Am. Chem. Soc. 106*, 2701-2703.

(22) DeClue, M. S., Baldridge, K. K., Künzler, D. E., Kast, P., and Hilvert, D. (2005) Isochorismate pyruvate lyase: A pericyclic reaction mechanism?, *J. Am. Chem. Soc. 127*, 15002-15003.

(23) Zhang, S., Pohnert, G., Kongsaeree, P., Wilson, D. B., Clardy, J., and Ganem, B. (1998) Chorismate mutase-prephenate dehydratase from *Escherichia coli*: Study of catalytic and regulatory domains using genetically engineered proteins, *J. Biol. Chem. 273*, 6248-6253.

(24) Liberles, J. S., Thórólfsson, M., and Martínez, A. (2005) Allosteric mechanisms in ACT domain containing enzymes involved in amino acid metabolism, *Amino Acids 28*, 1-12.

(25) Lütke-Eversloh, T., and Stephanopoulos, G. (2005) Feedback inhibition of chorismate mutase/prephenate dehydrogenase (TyrA) of *Escherichia coli*: Generation and characterization of tyrosine-insensitive mutants, *Appl. Environ. Microbiol. 71*, 7224-7228.

(26) Pittard, J., and Yang, J. (2008) Biosynthesis of the aromatic amino acids, *EcoSal Plus 3*, 1-39.

(27) Andrews, P. R., Smith, G. D., and Young, I. G. (1973) Transition-state stabilization and enzymic catalysis. Kinetic and molecular orbital studies of the rearrangement of chorismate to prephenate, *Biochemistry 12*, 3492-3498.

(28) MacBeath, G., Kast, P., and Hilvert, D. (1998) A small, thermostable, and monofunctional chorismate mutase from the archaeon *Methanococcus jannaschii*, *Biochemistry 37*, 10062-10073.

(29) Mattei, P., Kast, P., and Hilvert, D. (1999) *Bacillus subtilis* chorismate mutase is partially diffusion-controlled, *Eur. J. Biochem. 261*, 25-32.

(30) Sasso, S., Ramakrishnan, C., Gamper, M., Hilvert, D., and Kast, P. (2005) Characterization of the secreted chorismate mutase from the pathogen *Mycobacterium tuberculosis*, *FEBS J. 272*, 375-389.

(31) Helmstaedt, K., Heinrich, G., Lipscomb, W. N., and Braus, G. H. (2002) Refined molecular hinge between allosteric and catalytic domain determines allosteric regulation and stability of fungal chorismate mutase, *Proc. Natl. Acad. Sci. U. S. A. 99*, 6631-6636.

(32) Sasso, S., Ökvist, M., Roderer, K., Gamper, M., Codoni, G., Krengel, U., and Kast, P. (2009) Structure and function of a complex between chorismate mutase and DAHP synthase: Efficiency boost for the junior partner, *EMBO J. 28*, 2128-2142.

(33) Jiao, W., Hutton, R. D., Cross, P. J., Jameson, G. B., and Parker, E. J. (2012) Dynamic cross-talk among remote binding sites: The molecular basis for unusual synergistic allostery, *J. Mol. Biol. 415*, 716-726.

(34) Blackmore, N. J., Reichau, S., Jiao, W., Hutton, R. D., Baker, E. N., Jameson, G. B., and Parker, E. J. (2013) Three sites and you are out: Ternary synergistic allostery controls aromatic amino acid biosynthesis in *Mycobacterium tuberculosis*, *J. Mol. Biol. 425*, 1582-1592.

(35) Blackmore, N. J., Nazmi, A. R., Hutton, R. D., Webby, M. N., Baker, E. N., Jameson, G. B., and Parker, E. J. (2015) Complex formation between two biosynthetic enzymes modifies the allosteric regulatory properties of both: An example of molecular symbiosis, *J. Biol. Chem. 290*, 18187-18198.

(36) Munack, S., Roderer, K., Ökvist, M., Kamarauskaite, J., Sasso, S., van Eerde, A., Kast, P., and Krengel, U. (2016) Remote control by inter-enzyme allostery: A novel paradigm for regulation of the shikimate pathway, *J. Mol. Biol. 428*, 1237-1255.

(37) Roderer, K., Neuenschwander, M., Codoni, G., Sasso, S., Gamper, M., and Kast, P. (2014) Functional mapping of protein-protein interactions in an enzyme complex by directed evolution, *PLoS One 9*, e116234.

(38) Jiao, W., Blackmore, N. J., Nazmi, A. R., and Parker, E. J. (2017) Quaternary structure is an essential component that contributes to the sophisticated allosteric regulation mechanism in a key enzyme from *Mycobacterium tuberculosis*, *PLoS One 12*, e0180052.

(39) Kern, D., and Zuiderweg, E. R. P. (2003) The role of dynamics in allosteric regulation, *Curr. Opin. Struct. Biol. 13*, 748-757.

(40) Popovych, N., Sun, S., Ebright, R. H., and Kalodimos, C. G. (2006) Dynamically driven protein allostery, *Nat. Struct. Mol. Biol. 13*, 831-838.

(41) Tsai, C.-J., del Sol, A., and Nussinov, R. (2008) Allostery: Absence of a change in shape does not imply that allostery is not at play, *J. Mol. Biol. 378*, 1-11.

(42) Boehr, D. D., Nussinov, R., and Wright, P. E. (2009) The role of dynamic conformational ensembles in biomolecular recognition, *Nat. Chem. Biol. 5*, 789-796.

(43) Ferreon, A. C. M., Ferreon, J. C., Wright, P. E., and Deniz, A. A. (2013) Modulation of allostery by protein intrinsic disorder, *Nature 498*, 390-394.

(44) Nussinov, R., and Tsai, C.-J. (2015) Allostery without a conformational change? Revisiting the paradigm, *Curr. Opin. Struct. Biol. 30*, 17-24.

(45) Ikeda, M., and Nakagawa, S. (2003) The *Corynebacterium glutamicum* genome: Features and impacts on biotechnological processes, *Appl. Microbiol. Biotechnol. 62*, 99-109.

(46) Hermann, T. (2003) Industrial production of amino acids by coryneform bacteria, *J. Biotechnol. 104*, 155-172.

(47) Inui, M., Murakami, S., Okino, S., Kawaguchi, H., Vertès, A. A., and Yukawa, H. (2004) Metabolic analysis of *Corynebacterium glutamicum* during lactate and succinate productions under oxygen deprivation conditions, *J. Mol. Microbiol. Biotechnol. 7*, 182-196.

(48) Becker, J., and Wittmann, C. (2012) Bio-based production of chemicals, materials and fuels - *Corynebacterium glutamicum* as versatile cell factory, *Curr. Opin. Biotechnol. 23*, 631-640.

(49) Kalinowski, J., Bathe, B., Bartels, D., Bischoff, N., Bott, M., Burkovski, A., Dusch, N., Eggeling, L., Eikmanns, B. J., Gaigalat, L., Goesmann, A., Hartmann, M., Huthmacher, K., Krämer, R., Linke, B., McHardy, A. C., Meyer, F., Möckel, B., Pfefferle, W., Pühler, A., Rey, D. A., Rückert, C., Rupp, O., Sahm, H., Wendisch, V. F., Wiegräbe, I., and Tauch, A. (2003) The complete *Corynebacterium glutamicum* ATCC 13032 genome sequence and its impact on the production of L-aspartate-derived amino acids and vitamins, *J. Biotechnol. 104*, 5-25.

(50) Liu, Y.-J., Li, P.-P., Zhao, K.-X., Wang, B.-J., Jiang, C.-Y., Drake, H. L., and Liu, S.-J. (2008) *Corynebacterium glutamicum* contains 3-deoxy-D-*arabino*-heptulosonate 7-phosphate synthases that display novel biochemical features, *Appl. Environ. Microbiol. 74*, 5497-5503.

(51) Liebl, W., Ehrmann, M., Ludwig, W., and Schleifer, K. H. (1991) Transfer of *Brevibacterium divaricatum* DSM 20297^{T}, "*Brevibacterium flavum*" DSM 20411,

"*Brevibacterium lactofermentum*" DSM 20412 and DSM 1412, and *Corynebacterium lilium* DSM 20137^T to *Corynebacterium glutamicum* and their distinction by rRNA gene restriction patterns, *Int. J. Syst. Bacteriol. 41*, 255-260.

(52) Shiio, I., and Sugimoto, S. (1979) Two components of chorismate mutase in *Brevibacterium flavum*, *J. Biochem. 86*, 17-25.

(53) Sugimoto, S., and Shiio, I. (1980) Purification and properties of dissociable chorismate mutase from *Brevibacterium flavum*, *J. Biochem. 88*, 167-176.

(54) Li, P.-P., Liu, Y.-J., and Liu, S.-J. (2009) Genetic and biochemical identification of the chorismate mutase from *Corynebacterium glutamicum*, *Microbiology 155*, 3382-3391.

(55) Li, P.-P., Li, D.-F., Liu, D., Liu, Y.-M., Liu, C., and Liu, S.-J. (2013) Interaction between DAHP synthase and chorismate mutase endows new regulation on DAHP synthase activity in *Corynebacterium glutamicum*, *Appl. Microbiol. Biotechnol. 97*, 10373-10380.

(56) MacBeath, G., and Kast, P. (1998) UGA read-through artifacts—When popular gene expression systems need a pATCH, *Biotechniques 24*, 789-794.

(57) Grisostomi, C., Kast, P., Pulido, R., Huynh, J., and Hilvert, D. (1997) Efficient *in vivo* synthesis and rapid purification of chorismic acid using an engineered *Escherichia coli* strain, *Bioorg. Chem. 25*, 297-305.

(58) Smith, W. W., and Bartlett, P. A. (1993) An improved synthesis of the transition-state analog inhibitor of chorismate mutase, *J. Org. Chem. 58*, 7308-7309.

(59) Kabsch, W. (2010) *XDS*, *Acta Crystallogr. D Biol. Crystallogr. 66*, 125-132.

(60) Evans, P. R., and Murshudov, G. N. (2013) How good are my data and what is the resolution?, *Acta Crystallogr. D Biol. Crystallogr. 69*, 1204-1214.

(61) Karplus, P. A., and Diederichs, K. (2012) Linking crystallographic model and data quality, *Science 336*, 1030-1033.

(62) Diederichs, K., and Karplus, P. A. (2013) Better models by discarding data?, *Acta Crystallogr D 69*, 1215-1222.

(63) Karplus, P. A., and Diederichs, K. (2015) Assessing and maximizing data quality in macromolecular crystallography, *Curr. Opin. Struct. Biol. 34*, 60-68.

(64) McCoy, A. J., Grosse-Kunstleve, R. W., Adams, P. D., Winn, M. D., Storoni, L. C., and Read, R. J. (2007) *Phaser* crystallographic software, *J. Appl. Crystallogr. 40*, 658-674.

(65) Webby, C. J., Baker, H. M., Lott, J. S., Baker, E. N., and Parker, E. J. (2005) The structure of 3-deoxy-D-*arabino*-heptulosonate 7-phosphate synthase from *Mycobacterium tuberculosis* reveals a common catalytic scaffold and ancestry for type I and type II enzymes, *J. Mol. Biol. 354*, 927-939.

(66) Stein, N. (2008) *CHAINSAW*: a program for mutating pdb files used as templates in molecular replacement, *J. Appl. Crystallogr. 41*, 641-643.

(67) Emsley, P., Lohkamp, B., Scott, W. G., and Cowtan, K. (2010) Features and development of *Coot*, *Acta Crystallogr. D Biol. Crystallogr. 66*, 486-501.

(68) Murshudov, G. N., Vagin, A. A., and Dodson, E. J. (1997) Refinement of macromolecular structures by the maximum-likelihood method, *Acta Crystallogr. D Biol. Crystallogr. 53*, 240-255.

(69) Winn, M. D., Ballard, C. C., Cowtan, K. D., Dodson, E. J., Emsley, P., Evans, P. R., Keegan, R. M., Krissinel, E. B., Leslie, A. G. W., McCoy, A., McNicholas, S. J., Murshudov, G. N., Pannu, N. S., Potterton, E. A., Powell, H. R., Read, R. J., Vagin, A., and Wilson, K. S. (2011) Overview of the *CCP4* suite and current developments, *Acta Crystallogr. D Biol. Crystallogr. 67*, 235-242.

(70) Berman, H. M., Westbrook, J., Feng, Z., Gilliland, G., Bhat, T. N., Weissig, H., Shindyalov, I. N., and Bourne, P. E. (2000) The Protein Data Bank, *Nucleic Acids Res. 28*, 235-242.

(71) Velankar, S., Alhroub, Y., Alili, A., Best, C., Boutselakis, H. C., Caboche, S., Conroy, M. J., Dana, J. M., van Ginkel, G., Golovin, A., Gore, S. P., Gutmanas, A., Haslam, P., Hirshberg, M., John, M., Lagerstedt, I., Mir, S., Newman, L. E., Oldfield, T. J., Penkett, C. J., Pineda-Castillo, J., Rinaldi, L., Sahni, G., Sawka, G., Sen, S., Slowley, R., da Silva, A. W. S., Suarez-Uruena, A., Swaminathan, G. J., Symmons, M. F., Vranken, W. F., Wainwright, M., and Kleywegt, G. J. (2011) PDBe: Protein Data Bank in Europe, *Nucleic Acids Res. 39*, D402-D410.

(72) Krissinel, E., and Henrick, K. (2007) Inference of macromolecular assemblies from crystalline state, *J. Mol. Biol. 372*, 774-797.

(73) Schubert, O. T., Ludwig, C., Kogadeeva, M., Zimmermann, M., Rosenberger, G., Gengenbacher, M., Gillet, L. C., Collins, B. C., Röst, H. L., Kaufmann, S. H. E., Sauer,

U., and Aebersold, R. (2015) Absolute proteome composition and dynamics during dormancy and resuscitation of *Mycobacterium tuberculosis*, *Cell Host & Microbe 18*, 96-108.

(74) Shiio, I., and Sugimoto, S. (1981) Effect of enzyme concentration on regulation of dissociable chorismate mutase in *Brevibacterium flavum*, *J. Biochem. 89*, 1483-1492.

(75) Kubota, T., Tanaka, Y., Takemoto, N., Watanabe, A., Hiraga, K., Inui, M., and Yukawa, H. (2014) Chorismate-dependent transcriptional regulation of quinate/shikimate utilization genes by LysR-type transcriptional regulator QsuR in *Corynebacterium glutamicum*: carbon flow control at metabolic branch point, *Mol. Microbiol. 92*, 356-368.

(76) Bennett, B. D., Kimball, E. H., Gao, M., Osterhout, R., Van Dien, S. J., and Rabinowitz, J. D. (2009) Absolute metabolite concentrations and implied enzyme active site occupancy in *Escherichia coli*, *Nat. Chem. Biol. 5*, 593-599.

(77) Hagino, H., and Nakayama, K. (1975) Regulatory properties of chorismate mutase from *Corynebacterium glutamicum*, *Agric. Biol. Chem. 39*, 331-342.

(78) Kim, S.-K., Reddy, S. K., Nelson, B. C., Robinson, H., Reddy, P. T., and Ladner, J. E. (2008) A comparative biochemical and structural analysis of the intracellular chorismate mutase (Rv0948c) from *Mycobacterium tuberculosis* $H_{37}R_v$ and the secreted chorismate mutase (y2828) from *Yersinia pestis*, *FEBS J. 275*, 4824-4835.

(79) Kast, P., Asif-Ullah, M., Jiang, N., and Hilvert, D. (1996) Exploring the active site of chorismate mutase by combinatorial mutagenesis and selection: The importance of electrostatic catalysis, *Proc. Natl. Acad. Sci. U. S. A. 93*, 5043-5048.

(80) Burschowsky, D., van Eerde, A., Ökvist, M., Kienhöfer, A., Kast, P., Hilvert, D., and Krengel, U. (2014) Electrostatic transition state stabilization rather than reactant destabilization provides the chemical basis for efficient chorismate mutase catalysis, *Proc. Natl. Acad. Sci. U. S. A. 111*, 17516-17521.

(81) Burschowsky, D., Krengel, U., Uggerud, E., and Balcells, D. (2017) Quantum chemical modeling of the reaction path of chorismate mutase based on the experimental substrate/product complex, *Febs Open Bio 7*, 789-797.

(82) Webby, C. J., Jiao, W., Hutton, R. D., Blackmore, N. J., Baker, H. M., Baker, E. N., Jameson, G. B., and Parker, E. J. (2010) Synergistic allostery, a sophisticated regulatory network for the control of aromatic amino acid biosynthesis in *Mycobacterium tuberculosis*, *J. Biol. Chem. 285*, 30567-30576.

(83) Reichau, S., Jiao, W., Walker, S. R., Hutton, R. D., Baker, E. N., and Parker, E. J. (2011) Potent inhibitors of a shikimate pathway enzyme from *Mycobacterium tuberculosis:* Combining mechanism- and modeling-based design, *J. Biol. Chem. 286*, 16197-16207.

(84) Reichau, S., Blackmore, N. J., Jiao, W., and Parker, E. J. (2016) Probing the sophisticated synergistic allosteric regulation of aromatic amino acid biosynthesis in *Mycobacterium tuberculosis* using D-amino acids, *PLoS One 11*, e0152723.

(85) Schmidheini, T., Sperisen, P., Paravicini, G., Hütter, R., and Braus, G. (1989) A single point mutation results in a constitutively activated and feedback-resistant chorismate mutase of *Saccharomyces cerevisiae*, *J. Bacteriol. 171*, 1245-1253.

(86) Schnappauf, G., Lipscomb, W. N., and Braus, G. H. (1998) Separation of inhibition and activation of the allosteric yeast chorismate mutase, *Proc. Natl. Acad. Sci. U. S. A. 95*, 2868-2873.

(87) Kuroki, G. W., and Conn, E. E. (1988) Purification and characterization of an inducible aromatic amino acid-sensitive form of chorismate mutase from *Solanum tuberosum* L Tubers, *Arch. Biochem. Biophys. 260*, 616-621.

(88) Benesova, M., and Bode, R. (1992) Chorismate mutase isoforms from seeds and seedlings of *Papaver somniferum*, *Phytochemistry 31*, 2983-2987.

(89) Wendisch, V. F., Jorge, J. M. P., Pérez-García, F., and Sgobba, E. (2016) Updates on industrial production of amino acids using *Corynebacterium glutamicum*, *World J. Microbiol. Biotechnol. 32*, 105.

(90) Luttik, M. A. H., Vuralhan, Z., Suir, E., Braus, G. H., Pronk, J. T., and Daran, J. M. (2008) Alleviation of feedback inhibition in *Saccharomyces cerevisiae* aromatic amino acid biosynthesis: Quantification of metabolic impact, *Metab. Eng. 10*, 141-153.

SUPPLEMENTARY INFORMATION

Inter-enzyme allosteric regulation of chorismate mutase in *Corynebacterium glutamicum*: Structural basis of feedback activation by Trp

Daniel Burschowsky[1,†,§], Helen V. Thorbjørnsrud[1,§], Joel B. Heim[1], Jūratė Fahrig-Kamarauskaitė[2], Kathrin Würth-Roderer[2], Peter Kast[2*], Ute Krengel[1*]

[1] *Department of Chemistry, University of Oslo, NO-0315 Oslo, Norway*

[2] *Laboratory of Organic Chemistry, ETH Zurich, CH-8093 Zurich, Switzerland*

[†] *Present address: D. Burschowsky, Leicester Institute of Structural and Chemical Biology, University of Leicester, Leicester, UK*

[§] *These authors contributed equally to this work.*

**Corresponding authors*: P Kast, Laboratory of Organic Chemistry, ETH Zurich, HCI F 333, Vladimir-Prelog-Weg 3, CH-8093 Zurich, Switzerland; Tel.: +41 44 632 2908; E-mail: kast@org.chem.ethz.ch and U Krengel, Department of Chemistry, University of Oslo, Sem Sælandsvei 26, NO-0371 Oslo, Norway. Tel.: +47 22 85 5461; E-mail: ute.krengel@kjemi.uio.no.

SUPPLEMENTARY FIGURES

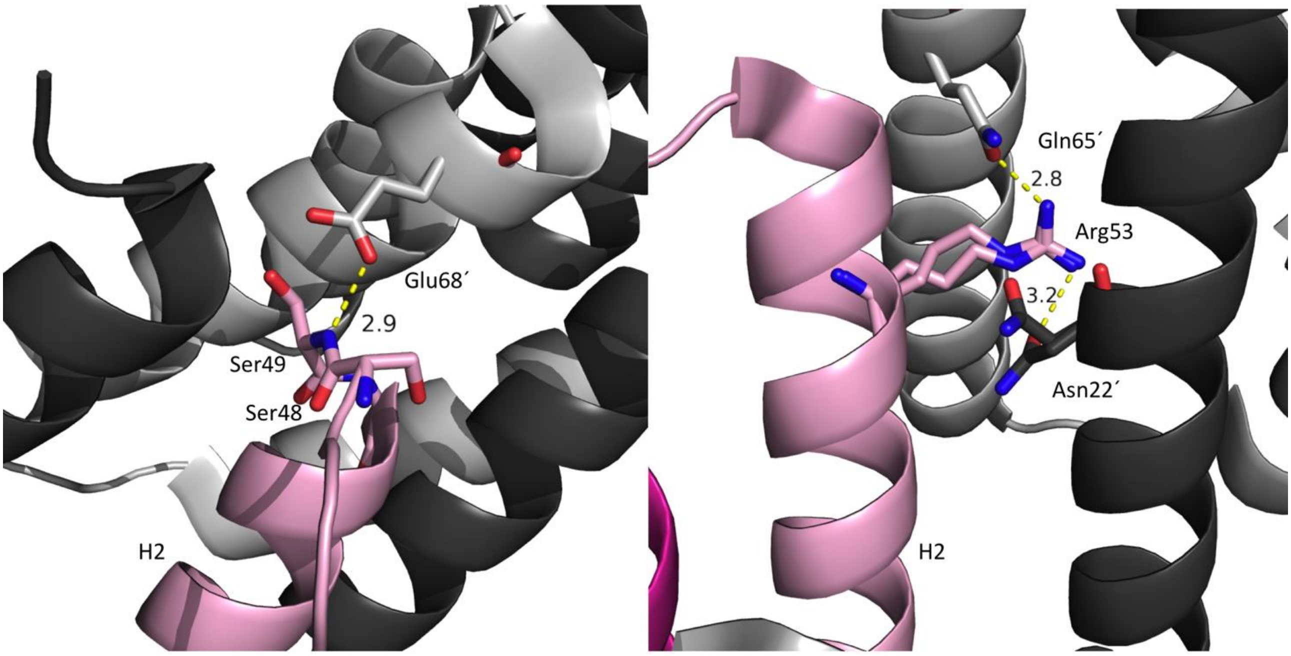

Supplementary Figure S1. Crystal contacts in apo CgCM. The two panels show interactions of the CgCM (PDB ID: 5HUB, this work) H2 helix (close to the H1-H2 loop) to the symmetry related molecules in the crystal. The reference CgCM homodimer is shown in shades of pink, and the symmetry related molecules in shades of grey.

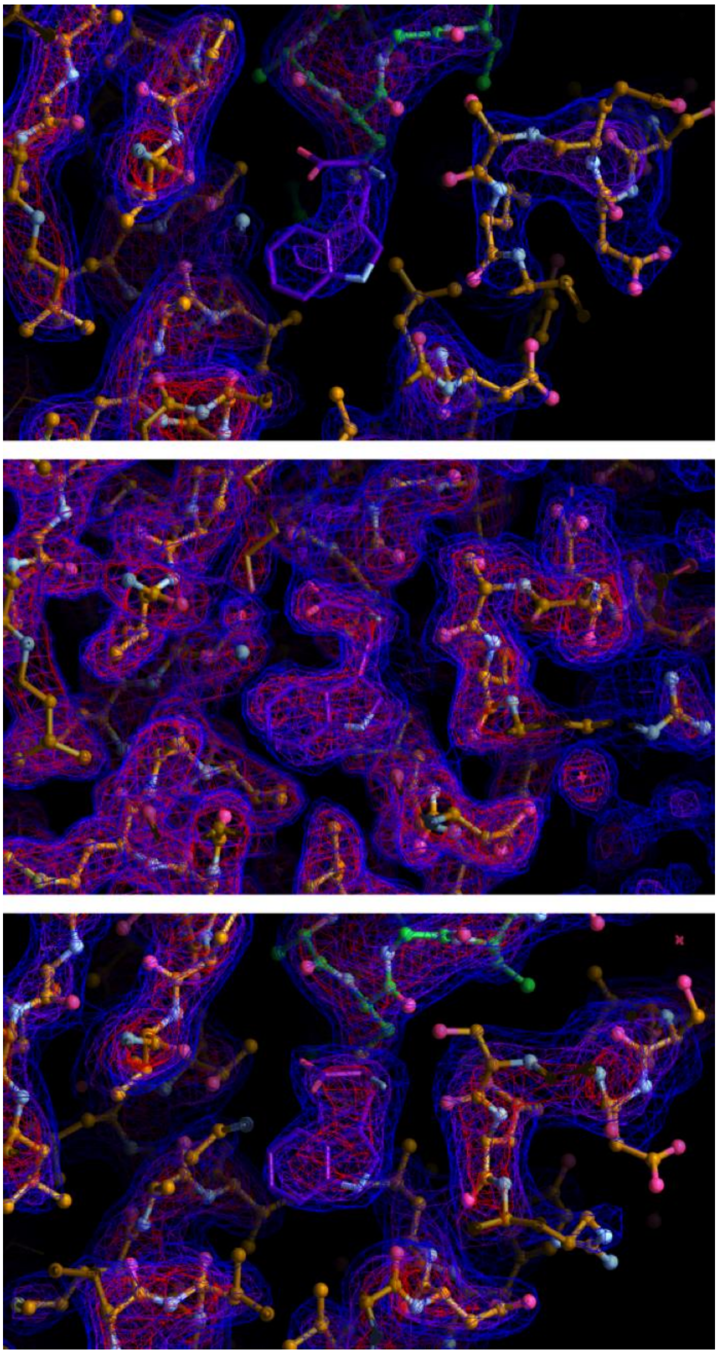

Supplementary Figure S2. Comparison of electron density in CgDS Trp binding pockets. Top: CgDS "apo" structure (PDB ID: 5HUC, this work, 2.5 Å resolution). Middle: CgCM-CgDS complex (chain A, PDB ID: 5HUD, this work, 2.2 Å resolution). Bottom: CgDS Trp soak (PDB ID: 5HUE, this work, 2.6 Å resolution). The σ_A-weighted $2F_o - F_c$ maps are contoured at 0.1 e/Å^3 (blue), 0.2 e/Å^3 (purple) and 0.3 e/Å^3 (red) for each of the structures (we compared absolute values rather than relative sigma-cutoffs to avoid bias due to different solvent contents, which are 29% for the CgCM-CgDS complex and 47% for the two CgDS structures). Resolution and quality of the CgDS structures in top and bottom panels is comparable, and the Trp ligand is clearly present at higher occupancy in the Trp soak. The structure of the CgCM-CgDS complex (middle panel) is better defined, in line with its higher resolution, however, the electron density of Trp is incomplete and of lower quality than that of the interacting protein residues, suggesting lower occupancy of the binding site as in the Trp soak. We estimate that Trp occupancy in the non-soaked structures is approximately equal, which is supported by a *B*-factor analysis of interacting residues.

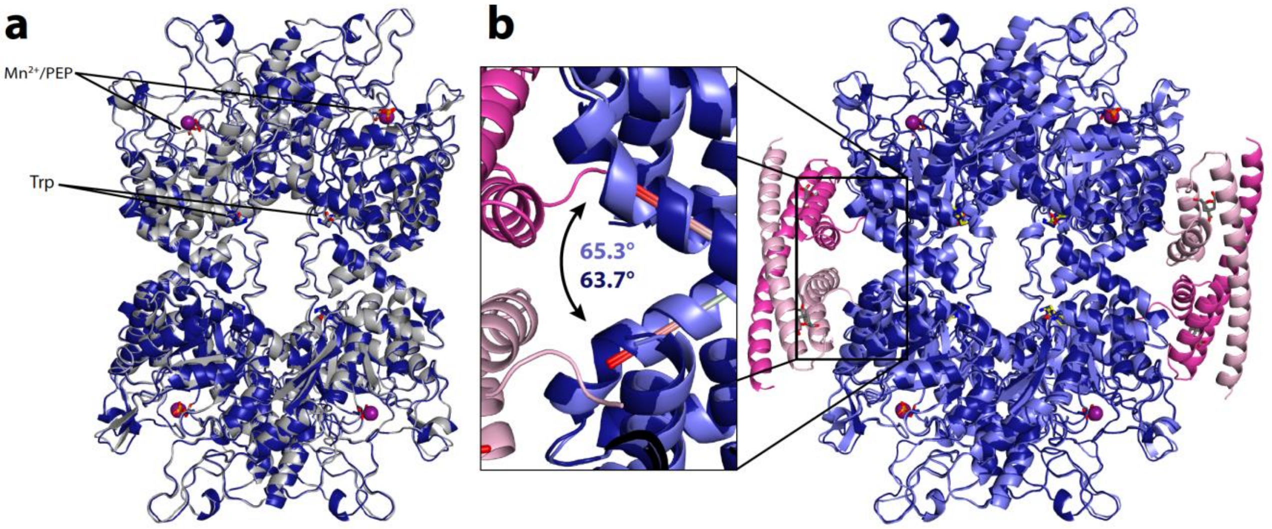

Supplementary Figure S3. Comparison of CgDS structures. (a) CgDS (light gray, PDB ID: 5HUC, this work) superimposed with the structure of the CgDS-Trp soak (dark blue, PDB ID: 5HUE, this work). The superimposition was performed over all backbone atoms of the CgDS tetramers. (b) CgCM-CgDS-complex (violet blue and pink, PDB ID: 5HUD, this work) superimposed with the CgDS-Trp soak shown in (a). Superimpositions were performed over all backbone atoms of the CgDS A chains (subunit in the upper right position). The boxed area shows a close-up view of the CgCM-CgDS interface. Upon complex formation with CgCM, CgDS subunits moved further apart (indicated by the double-headed arrow), showing a slightly different relative tetrameric alignment of CgDS subunits compared to CgDS alone (with or without additional Trp). The angles were measured between the helices formed by residues 225-239 (CgDS) of two adjacent subunits (*i.e.*, the angles between the helix axes, shown as sticks in the helix centers). Mn^{2+} ions are shown as purple spheres, PEP and Trp are shown as sticks.

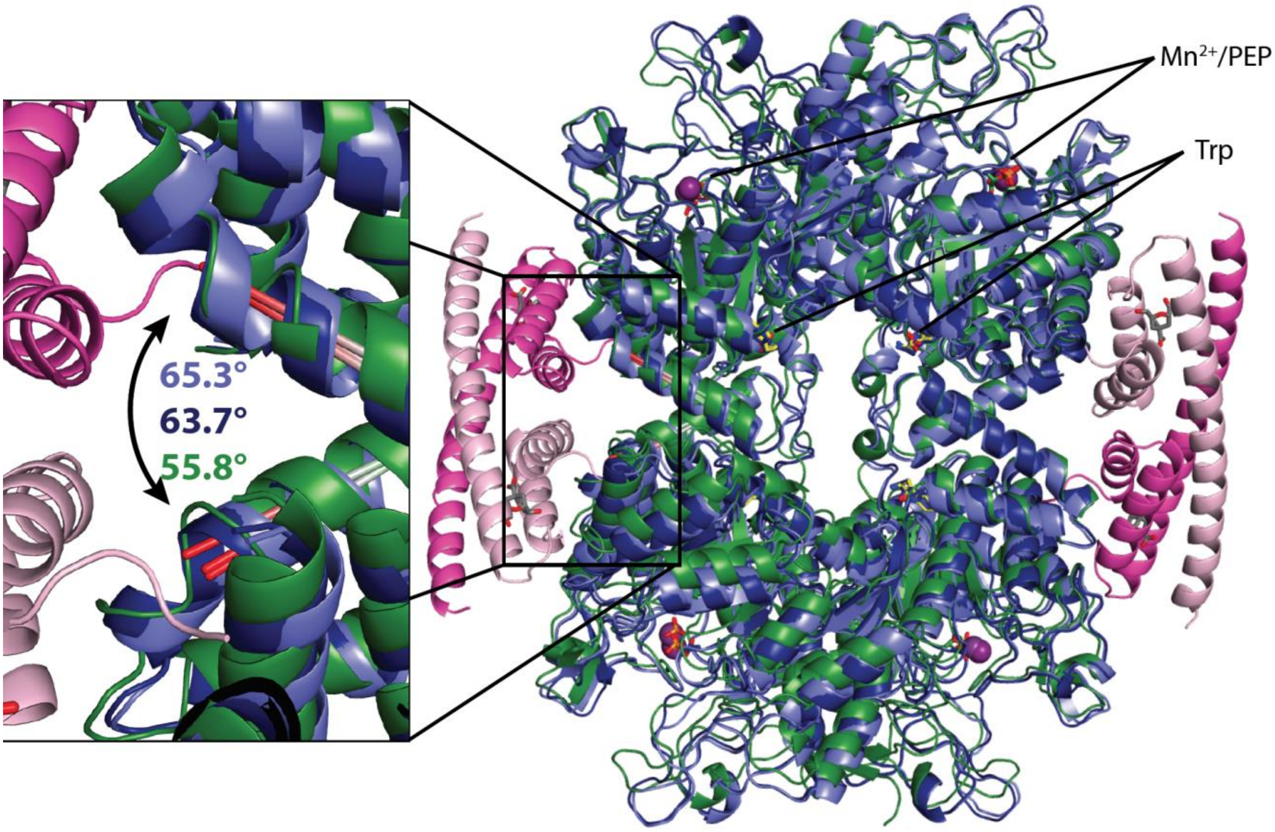

Supplementary Figure S4. Structural comparison of CgDS with MtDS. CgDS-Trp soak (dark blue, PDB ID: 5HUE, this work) superimposed with the MtDS apo structure (green, PDB-ID: 3NV8 (1)) and the CgDS-CgCM complex (violet blue and pink, PDB ID: 5HUD, this work). Superimpositions were performed over all backbone atoms of the CgDS A chain (subunit in the upper right position). The boxed area shows a close-up view of the binding interface for CM (double-headed arrow). The angles were measured between the helices formed by residues 215-229 (MtDS) or residues 225-239 (CgDS) of two adjacent subunits (*i.e.*, the angles between the helix axes, shown as sticks in the helix centers). The relative alignment of CgDS subunits in the Trp complex lies between that of the MtDS apo form and the CgDS complex with CgCM. Mn^{2+} ions are shown as purple spheres, PEP and Trp are shown as sticks.

SUPPLEMENTARY TABLE

CgDS - PDB ID 5HUE

Trp		ASA (Å²)	BSA (Å²)
TRP	1	355.3	290.5
TRP	1	355.3	57.6

CgDS		ASA (Å²)	BSA (Å²)
LEU	117	3.7	3.7
ALA	120	2.7	2.7
VAL	121	14.6	5.8
THR	124	54.0	14.6
PRO	130	86.6	4.4
VAL	131	9.9	4.7
LYS	133	33.4	28.6
ALA	202	4.3	4.3
LEU	204	43.9	29.1
LEU	207	6.9	6.9
SER	247	91.3	29.6
LEU	248	21.5	6.1
ALA	250	48.2	12.2
ALA	251	26.0	15.7
ASP	252	90.0	1.8
PHE	237	135.8	0.5
ALA	240	84.4	6.3
CYS	241	82.0	47.1
GLY	242	64.2	0.2

MtDS - PDB ID 3NUE

Trp	ASA (Å²)	BSA (Å²)
TRP9004	351.19	307.3
TRP9004	351.19	60.3

MtDS		ASA (Å²)	BSA (Å²)
LEU	107	6.4	6.3
ALA	110	2.7	2.7
VAL	111	13.1	7.5
THR	114	54.3	16.3
PRO	120	89.2	3.7
VAL	121	7.2	1.7
LYS	123	39.1	30.2
ALA	192	4.5	4.5
LEU	194	40.7	28.2
VAL	197	2.2	2.2
ASN	237	129.8	27.8
LEU	238	29.2	9.1
THR	240	60.3	8.7
ALA	241	26.0	15.1
GLU	242	67.6	1.0
PHE	227	136.7	0.5
ALA	230	86.6	6.1
CYS	231	84.0	50.3

Supplementary Table S1. Surface area of Trp interface in CgDS and MtDS. Surface area of the Trp ligand bound to either CgDS (PDB ID: 5HUE, this work) or MtDS (PDB ID: 3NUE, (1)), calculated per interacting residue. ASA = accessible surface area; BSA = buried surface area; interactions in the main binding pocket are shaded in green, interactions with the second subunit are shaded in yellow. The surface areas were calculated using the PDBe PISA Server (2).

SUPPLEMENTARY REFERENCES

1. Webby CJ, Jiao W, Hutton RD, Blackmore NJ, Baker HM, Baker EN, et al. Synergistic allostery, a sophisticated regulatory network for the control of aromatic amino acid biosynthesis in *Mycobacterium tuberculosis*. J Biol Chem. 2010;285(40):30567-76.

2. Krissinel E, Henrick K. Inference of macromolecular assemblies from crystalline state. J Mol Biol. 2007;372(3):774-97.